This manuscript was accepted by J. Appl. Phys. Click here to see the version of record.

Influence of pre-annealing of printed silver electrodes on ultrafast laser ablation of short thin-film transistor channels on flexible substrates

M.S. Wiig[1)], C. C. You[1)], C. Brox-Nilsen[2)] and S. E. Foss[1)]

[1)]*Solar Energy Department, Institute for Energy Technology, 2007 Kjeller, Norway*
[2)]*Thin Film Electronics ASA, 0230 Oslo, Norway*

The cutoff frequency and current from an organic thin-film transistor (OTFT) is strongly dependent on the length and to some extent the uniformity of the transistor channel. Reducing the channel length can improve the OTFT performance by increasing the current and frequency. Picosecond laser ablation of printed Ag electrodes, compatible with roll-to-roll fabrication has been investigated. The ablation threshold was found to be similar for the laser wavelengths tested: 515 nm and 1030 nm. Short transistor channels could be opened both after light annealing at 70ºC and after annealing at 140ºC. The channels in the lightly cured films had significantly less scale formation which critical for avoiding shunts in the device. By moving from bottom electrodes fully defined by printing to bottom electrodes where the transistor channel is opened by laser, the channel length could be reduced from 40 µm to less than 5 µm.

I. INTRODUCTION

The printed and flexible electronics industry is quickly emerging and a lot of research is focused on the topic. In recent years, there has been great interest in the use of organic thin-film transistor (OTFT) device technology in next-generation thin film electronics, due to the performance enhancements enabled by its use in applications such as flexible displays, large-area sensors, radio frequency identification (RFID) tags, and ultrathin electronics[1]. However, still commercial large scale production is in the initial phase and few products have reached their full potential in the market yet. The industry is currently expanding production.

To make more advanced printed circuit elements there is a request for better performance while still maintaining low cost. Compared to vacuum processes and photolithographic processes, fully printed organic thin-film transistor (OTFT) devices have challenges related to surface roughness, edge waviness of the patterns and poor registration accuracy of the drain-source electrodes to the gate electrode. This may generate OTFTs with large variation in threshold voltage[2], which gives fewer opportunities to fabricate commercially relevant integrated devices.

The channel length and the overlap between the drain-source electrodes with the gate are dominant factors in determining the cutoff frequency (f_t) of OTFTs, given by Eq. (1)

$$f_t \approx \frac{\mu_{eff}(V_{GS}-V_{th})}{2\pi(L^2+2LL_c)}, \quad (1)$$

where μ_{eff} is the effective charge carrier mobility, the channel length L is the distance between the source and drain electrode and L_c is the contact length (overlap between drain-source and gate electrode). V_{GS} is gate voltage and V_{th} is threshold voltage. A schematic illustration of the device structure is shown in Fig. 1.

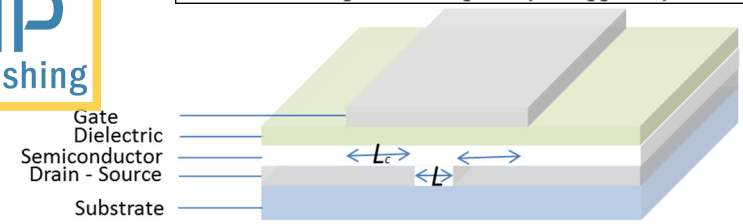

Fig. 1: Schematic illustration of an OTFT device structure.

For printed organic thin-film transistors (OTFT), the length of the channel between source and drain is a crucial parameter. A shorter channel allows for using higher operating frequencies, and increases the current throughput capacity. If the OTFTs are part of a ring oscillator the operating frequency has a quadratic dependence on the channel length, as indicated by Eq. 1[3] making this parameter even more important. Fully printed transistors with short channels have been achieved with inkjet printing technology. Similar channel lengths are not practically achieved with high throughput R2R processing. An alternative process to high resolution printing is subtractive laser ablation of the channel. Laser opening of channels can reduce the channel length and the uniformity is superior compared to R2R printed transistors where the edge definition often can be wave like. Laser direct writing (LDW) processes is compatible with integration in R2R production[4]. Laser ablated channels have previously been successfully achieved in combination with inkjet printing of nanoparticle ink[5,6].

Femtosecond (fs) and picosecond (ps) pulsed lasers have advantages over nanosecond (ns) pulsed lasers in the ability to achieve cold processing. For ns lasers ionization, sample heating, and vaporization all occur during the laser pulse. Fs and ps laser pulses are so short that these phenomena do not occur until the end or after the laser pulse. Femtosecond and picosecond pulse duration is shorter than the characteristic relaxation times, such as electron-to-ion energy transfer time, electron heat conduction time, and hydrodynamic or expansion time[7]. This makes ultrashort and short pulse lasers suitable for processing on heat sensitive substrates such as polymers used in printed electronics.

In this work we study the laser material interaction on films annealed at low temperature at 70 ºC, versus films annealed at 140 ºC and develop a process for damage free picosecond laser ablation of a short OTFT channel on an electrode printed from Ag precursor ink. In addition to a dependence on laser parameters; wavelength, repetition rate, fluence and speed, the quality of the laser opened channel strongly depends on the pre-annealing conditions.

II. EXPERIMENTAL

Bottom electrodes were flexo or gravure printed using sheet-fed printing machines. The electrode was printed as one 1.2 mm times 0.5 mm pad with two connectors, the large pad was then separated into source and drain electrodes by laser scribing, Fig. 2. The ink was a precursor Ag ink with a thickness of approximately 50-80 nm after annealing at 140ºC on a polyethylene naphthalate (PEN) substrate. To achieve good conductivity the film has to be annealed at high temperature (HT) 140 ºC for 10 minutes. Post-annealing the samples at HT after a low temperature (LT) annealing at 70 ºC for 10 minutes decreased the resistivity with approximately three orders of magnitude, compared to only LT annealing at 70 ºC. The annealing was performed under atmospheric conditions in a Thermaks heating cabinet.

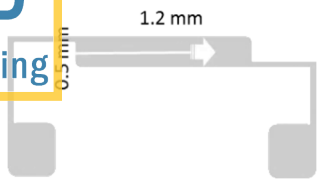

Fig. 2: Layout of drain - source electrode. The arrow indicates the path for laser patterning.

The laser ablation process was performed with an s-Pulse laser from Amplitude-Systems. The pulse duration was 3 ps at 1 kHz repetition rate. The pattern was outlined by movement of a xy-table, while using a stationary laser beam. The distance between the centers of two successive laser pulses is determined by the ratio of the speed of the xy-table and the repetition rate of the laser pulse. Two different laser beams with wavelengths of 1030 nm (IR) and 515 nm (VIS) were used. The 6 mm collimated beam was focused through a fixed lens with a focal length of 75 mm, the focused beam diameter was ~16 µm. The pulse energy was measured with a coherent PS19Q powermax sensor.

The laser material interaction has been investigated after LT annealing the ink at 70 °C for 10 minutes and after HT annealing at 140 °C for 10 minutes using both the 1030 nm and 515 nm wavelength laser beams. Optical microscopy images of the laser opened areas were acquired with a Zeiss axiovision imaging system. The samples for both annealing conditions were cut from the same print area, and both wavelengths were tested on the same two samples. This was done to avoid influence on the laser process of any large area inhomogeneity in the printing.

III. Results and discussion

A. Single spot ablation

Two important parameters describing the laser ablation process is the ablation threshold, i.e. the minimum energy density required to open the film, and the waist diameter of the beam.

The ablation threshold for single pulse ablation were calculated by Eq. 2 and 3 [8,9].

$$r^2 = \frac{\omega_0^2}{2} \ln \frac{\Phi_o}{\Phi_{th}}, \tag{2}$$

$$\Phi_0 = \frac{2E_{pulse}}{\pi \omega_0^2} \tag{3}$$

Where r is the radius of the opened spot, for the LT anneal the periphery of the ablated area was defined at the inner radius of the dark rim, Fig. 4 b) and d), and ω_o is the half width of the laser beam. The radius was measured from optical microscopy images of laser opened spots at different pulse energy (E_{pulse}). Φ_0 and Φ_{th} are the peak fluence and ablation threshold fluence respectively. The waist diameter of the beam (ω_o) is found from a linear regression of r^2 vs. ln E_{pulse} according to Eq 2 and 3, ($\omega_o = \sqrt{2 * slope}$). The fluence at the ablation threshold was found from the pulse energy where the linear fit of $r^2 = 0$.

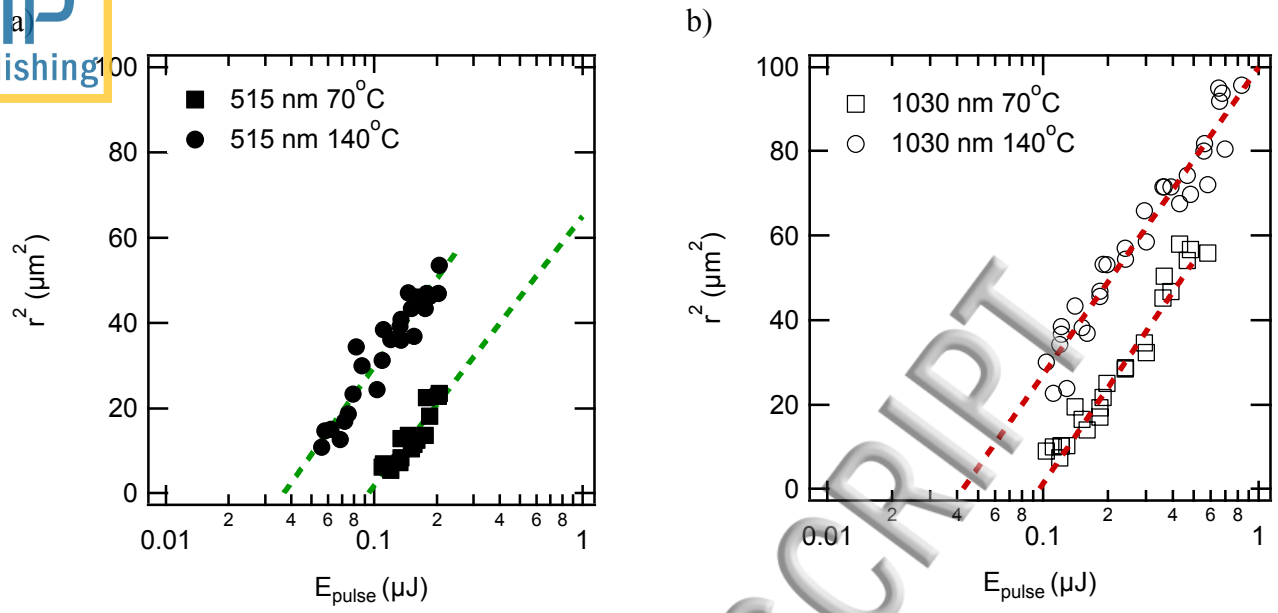

Fig. 3: r^2 of the laser opened area vs. pulse energy for printed Ag annealed at LT (squares) and HT (circles) with two laser wavelengths a) 515 nm and b) 1030 nm ablation

Table 1: Ablation threshold

Annealing temperature (°C)	Φ_{th} (J/cm^2) 515 nm	E_{th} (μJ) 515 nm	Φ_{th} (J/cm^2) 1030 nm	E_{th} (μJ) 1030 nm	Beam diameter (μm)
70	0.11±0.04	0.09±0.02	0.09±0.01	0.095±0.008	15
140	0.039±0.007	0.037±0.004	0.043±0.005	0.042±0.003	16

Fig. 3 a) and b) show r^2 vs. pulse energy for 515 and 1030 nm single spot laser ablation. After HT annealing the ablation threshold (Φ_{th}) was 0.04 J/cm^2 independent of wavelength, as shown in Table 1. For the LT annealed film Φ_{th} for 515 nm was 0.11 J/cm^2 and for 1030 nm Φ_{th} was 0.09 J/cm^2, which differed with less than one standard deviation. Hence for both annealing conditions there was no significant wavelength dependence of the ablation threshold. The ablation thresholds for the LT annealed samples were a factor 2-3 higher compared to the HT annealed sample. Different ablation threshold for sintered and non-sintered ink can be used to selectively ablate a multilayer structure, as demonstrated by Ko[10]. However contrary to the current study they observed a lower ablation threshold for sintered gold nano-particle ink compared to un-sintered ink. Laser annealing at laser powers below the ablation threshold can be used for direct sintering of conductive lines. This technique has been used to form highly conductive interconnects with nanosecond lasers [10-12].

Post annealing a sample at HT for 10 minutes after LT annealing for 10 minutes reduces the film thickness to about half. The high resistivity before the last HT anneal indicates that the lightly cured film was not fully sintered. The large change in thickness also indicates that the lightly cured film still contained a large amount of residual solvent. The additional energy required to evaporate the solvents[12] can explain the observed higher ablation threshold for the lightly annealed film compared to HT annealed film.

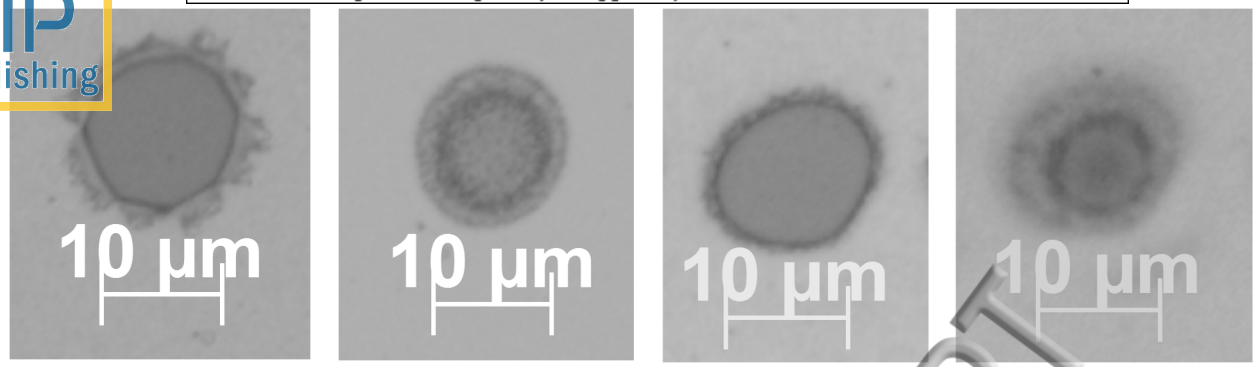

a) 1030 nm 140 °C 0.151 µJ | b) 1030 nm 70 °C 0.151 µJ | c) 515 nm 140 °C 0.146 µJ | d) 515 nm 70 °C 0.146 µJ

Fig. 4: shows light microscopy images of an annealed film at 140 °C or lightly annealed at 70 °C after interaction with a 1050 nm or 515 nm laser pulse.

For all four parameter sets it was possible to ablate the film without introducing considerable visible damage to the polymer substrate. Single spot laser ablation after HT annealing the Ag film Fig. 4 a) and c) results in sharp scale formation around the edges. Even though there is no significant difference in the ablation threshold for 515 and 1030 nm the visual appearance of the laser opened spots are different. The scale formation is more pronounced for the 1030 nm laser beam compared to 515, see images in Fig. 4 a) and c). After ablation residues from the film curl up around the edges, the height of these scales was measured to be around 2 µm, as revealed by non-contact atomic force microscopy (AFM) measurements. An AFM topography image and height profile is shown in Fig. 5.

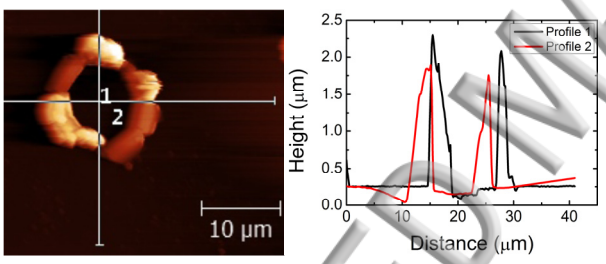

Fig. 5: AFM image and height profile of a laser opened spot with a pulse energy of 0.13µJ 1030 nm wavelength. The film was annealed 10 min at 140°C (HT).

The above mentioned influence of laser wavelength on the appearance of the laser opened spot is minor compared to the influence on the laser material interaction due to different pre-annealing of the film.

From these observations, the ablation mechanism of the film annealed at HT appears to be photo-induced laser spallation. The stresses and shockwaves generated in the film by laser irradiation lead to the disruption of the film/substrate interface[13,14]. This means that the film can be opened without strong thermal effects like evaporation or melting. The visual appearance of the edges is similar to that observed for metallic Pt and Ag films deposited by RF sputtering, opened with a 1030 nm 500 fs laser pulse[15]. As seen from Fig. 6 b, there is no proof of energy absorption in the substrate even at the highest powers tested for this film annealed at HT. One would expect such energy absorption would cause a change in the substrate surface appearance in microscope images, either by a melting and re-solidifying induced roughness or an uneven ablation of material.

This manuscript was accepted by J. Appl. Phys. Click here to see the version of record.

The two samples annealed at 70 °C (Fig. 4b and Fig. 4d) have a darker rim surrounding the laser opened area, but the transition is smooth without any scale formation. Outside this rim there is a region appearing slightly darker than the bulk film. The definition of the outer ring is slightly sharper for the 1030 nm ablation. The spot appearance after ablation with increasing pulse energy is shown in Fig. 6a) for the LT annealed film. The ablation mechanism can clearly be separated from mechanical spallation after HT anneal, Fig. 6 b. At LT the material removal seems to increase gradually with increasing pulse energy, and the dark rim next to the opened area, might be due to laser annealing of the film and/or evaporation of residual solvent by the power of the Gaussian beam profile below the ablation threshold. Particle removal may take place simultaneously with evaporation of residual solvents, and there can be some buildup of particles in the darker area. At increasing pulse energy a gradient with darker color toward the center was observed indicating that some of the energy is deposited in the substrate.

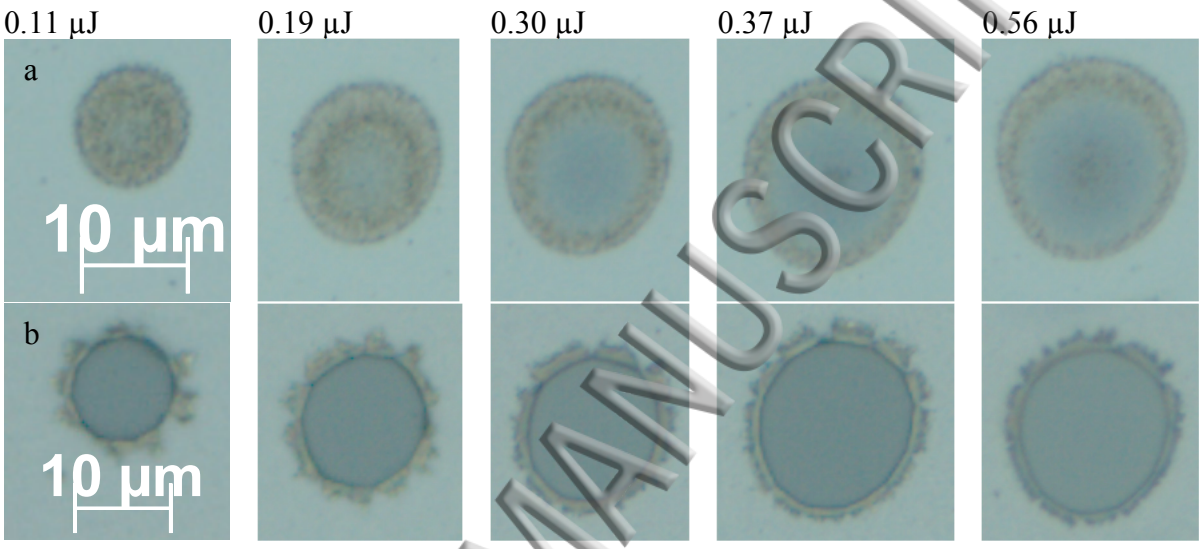

Fig. 6: 1030 nm laser ablated spots with increasing pulse energy from left to right pre-annealed at LT row a) and HT row b).

The different ablation mechanisms observed for the two films is expected to be related to different mechanical properties of the films after the two annealing treatments. The HT annealed film has high conductivity and formation of a continuous film is expected. During ablation all the energy is absorbed in the silver and this film will either be ruptured or removed as one piece. While in the LT anneal film some of the energy was absorbed by the solvents, and incomplete reaction of the precursor ink leaves a discontinuous film were particles evaporate together with the solvent.

B. Line ablation with overlapping spots annealed at 140 °C

At increasing spot to spot overlap a continuous laser opened line is formed where the outline of the single spots at the edges vanishes. The edges are still associated with severe scale formation. The width of the laser opened line increases with increasing power as a lager area of the beam has energy above the ablation limit. The width of the opened line follows the diameter of the single spots. The laser power required for opening single spots and full lines are similar for the film annealed at HT. Fig. 7 (1030 nm) and Fig. 8 (515 nm) shows the laser opened lines with increasing spot to spot overlap from top to bottom and increasing fluence from b) to e).

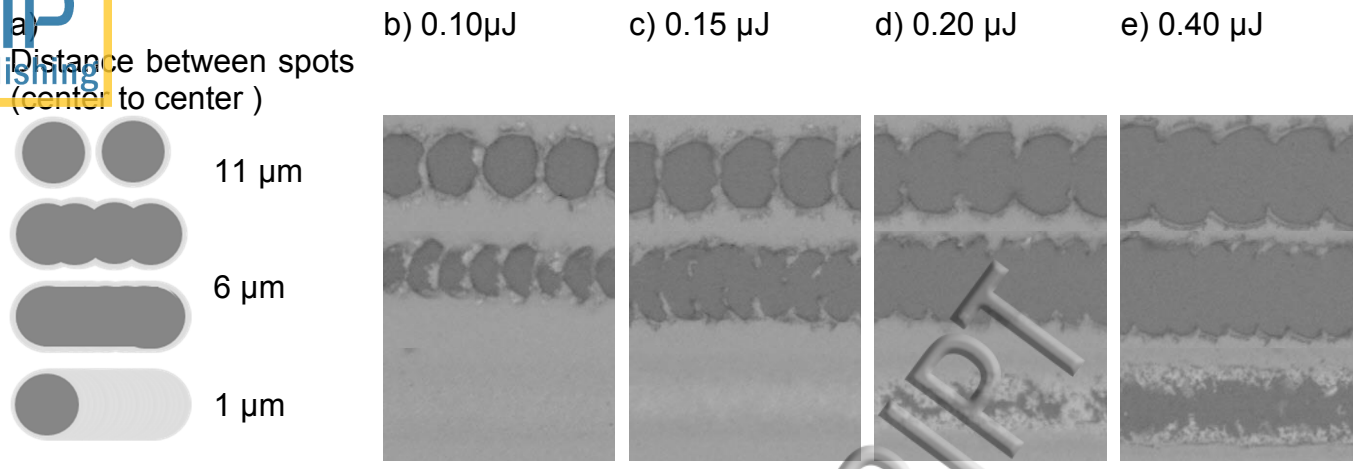

Fig. 7: 1030 nm annealed at 140 ºC

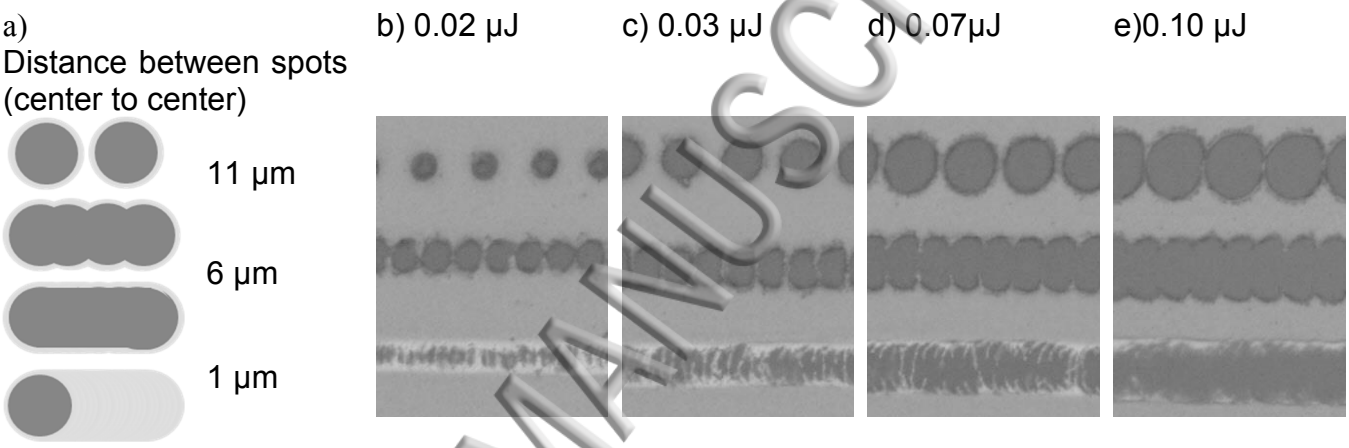

Fig. 8: 515 nm annealed at 140 ºC

At very large overlap with a distance of ~1 μm between the centers of two successive spots, no line is opened even if the fluence is sufficient for single spot ablation. Instead a bright laser annealed line can be observed where only the first pulse has opened through the film, Fig. 9b) and Fig. 10a). At increasing laser fluence the film cracks open as seen in Fig. 9c). This annealing is observed for both laser beams and both thermal treatments, however the cracking of the film is only observed after HT anneal. On the LT annealed sample increased particle removal are observed when moving out of the parameter range for laser annealing by increasing spot to spot distance, shown in Fig. 10 b, or increasing laser power. Increased resistance against laser ablation at increasing spot to spot overlap can be explained due to the annealed ring surrounding a single laser opened spot. This ring is seen most clearly in the images of lightly annealed samples in Fig.4 b) and d) where the area surrounding the opened spot, which is exposed to a laser power below the ablation threshold, is annealed. If the subsequent laser pulse overlaps with this annealed ring from the previous pulse rather than a fresh area, the ablation threshold is higher and the annealed ring is not opened by the subsequent pulse. The pulse still anneals a new outer ring pushing the front forward forming a continuous laser annealed line. This principle is illustrated in Fig. 9a). Even though the ablation threshold was found to be higher for the lightly annealed film with residual solvents, the ablation threshold of an annealed film at 140ºC increases upon additional laser annealing.

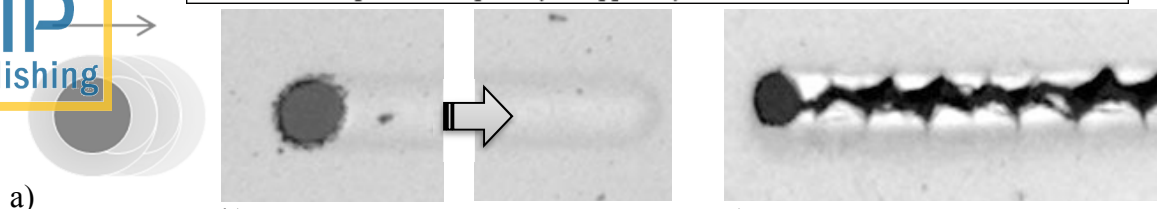

Fig. 9: Laser annealed front at high spot to spot overlap on HT annealed Ag print.

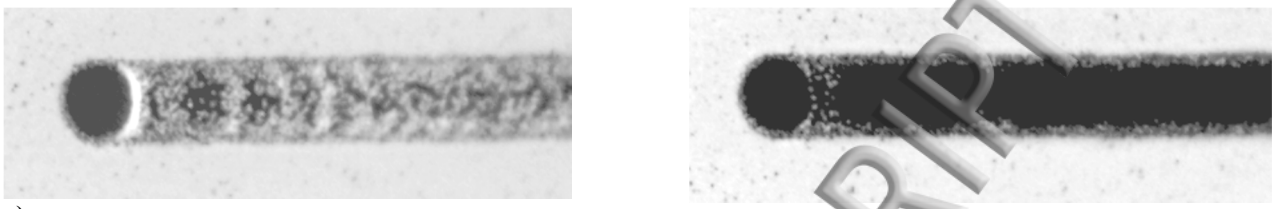

Fig. 10: Laser annealed line with 515 nm on LT annealed substrate, with spot to spot center distance of a) 0.2 µm and b) 0.4µm.

As seen from Fig. 10 a) also on the LT annealed film a slow beam speed causes pre-annealing of the line before the successive pulse, increasing the ablation threshold compared to fast processing, Fig. 10b). However the line was porous due to a limited power range separating annealing and onset of evaporation of particles as has also been observed by pulsed laser sintering of wet ink.[12] In accordance with our observations of increased removal of particles with increasing speed they also observed too fast sintering to cause porous lines.

C. Laser opening of lightly annealed films

Continuous lines could be opened with both wavelengths on the lightly annealed samples at 70 ºC shown in Fig. 11b). The edges appear smooth without any scale formation as were observed on the samples annealed at 140 ºC, Fig. 7 and Fig. 8.

For a wavelength of 515 nm the width of the laser opened line can be tuned below the half width of the beam by reducing the power such that only the center peak of the beam has energy above the ablation limit. Well defined lines of 5 µm with smooth edges could be scribed with the 515 nm beam on lightly annealed Ag prints. Linewidths in the range 4-15 µm could be obtained without visually damaging the polymer substrate, resulting from a variation of the pulse energy by one order of magnitude. At pulse energies above 0.3 µJ damage to the polymer substrate could be observed.

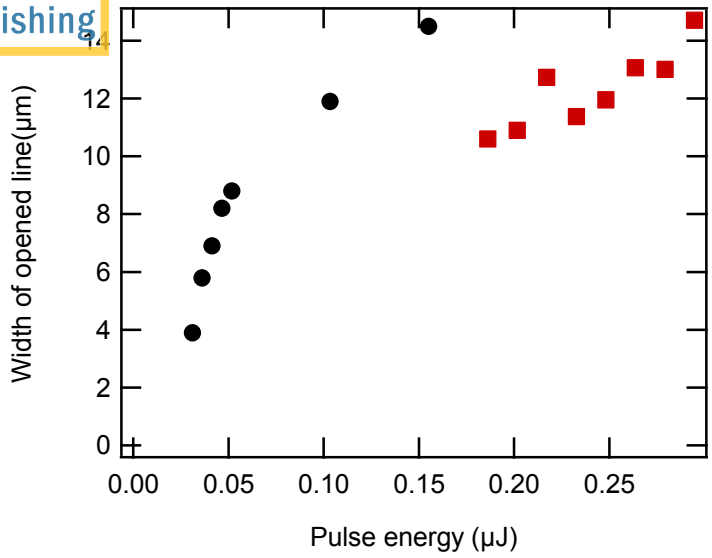

Fig. 11: Laser (515 nm) ablated linewidth (circles) and ablated spot diameter (squares) for the 515 nm, beam vs. pulse energy at LT annealed film. The center to center spot distance of the lines were 1 μm.

Fig. 11 shows the linewidth and single spot diameter vs. laser pulse energy. The minimum pulse energy for opening continuous lines is smaller than that for single spot ablation, indicating interaction between multiple pulses, so called incubation effects. This applies at larger spot to spot distance than the laser annealing described above. These interactions between multiple pulses also enable scribing of lines that are narrower than the minimum size of a single laser opened spot. For the laser beam with 1030 nm the minimum linewidth was limited to the beam diameter, as the pulse energy for 1030 nm could not be attenuated below 0.1 μJ.

Fig. 12 shows images of laser opened lines as a function of speed and power. Both for low spot to spot overlap and very high spot to spot overlap the width of the laser opened line is reduced and the edges becomes less well defined compared to the intermediate speeds. In the case of high overlap the cause is pre-annealing by the previous laser spot, which was also observed for the fully annealed films. In the lightly annealed samples this appears as particles of residue in the channel, and a rough edge with small particles attached. In the case of too high speeds the reduced incubation effects narrows down the laser opened area to approach the width of a single spot. In this case the contour of the circular beam becomes visible along the edge at small spot to spot overlap.

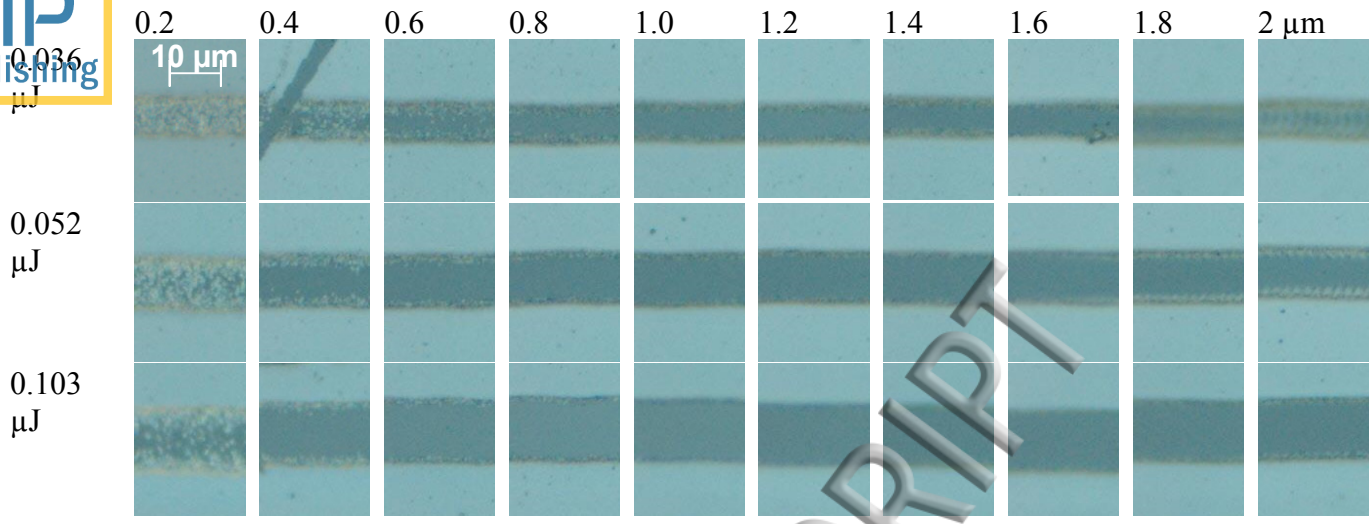

Fig. 12: Laser opened lines with 515 nm at 1 kHz, the Ag print was annealed at 70 ºC for 10 min. Increasing pulse energy from top to bottom, and spot to spot distance from left to right (center to center distance).

D. Scribing narrow TFT channels

The above developed process for scribing narrow lines on lightly annealed Ag-prints, results in well-defined lines with only minor variations in the linewidth. Fig. 13 shows images of a fully printed bottom electrode in comparison with a laser patterned electrode. For the fully printed electrode the variation in channel length along the width of the channel is larger than the total length of the laser processed channel. By shifting from fully printed source and drain electrodes to a laser opened channel between the electrodes the dimensions of the channel can be reduced from 40 µm to 5 µm. Improved performance of the transistor can be expected by introducing this process for separating the source and drain electrodes.

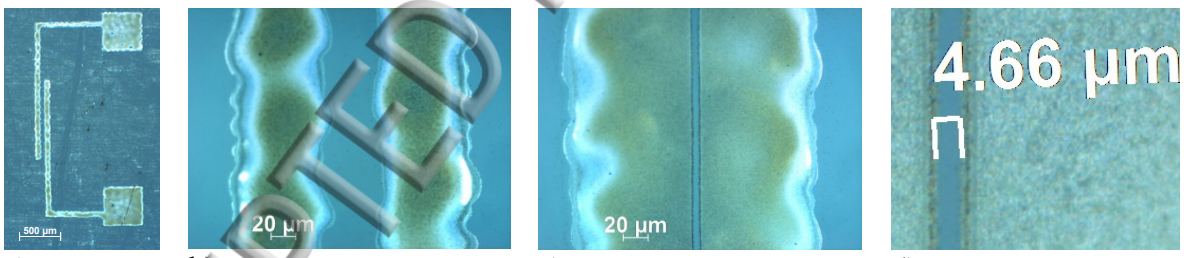

a) b) c) d)

Fig. 13: Separating OTFT drain-source bottom electrodes. a) drain-source electrode layout b) fully printed channel c) laser opened channel d) laser opened channel.

However, narrowing the channel also contributes to the short channel effect with pronounced contact resistances, which limits the operating frequencies. To overcome the short channel issue, the ratio of gate dielectric thickness (d) and channel length (L) should follow, $d/L \leq 0.25$[3]. As well defined short channels of a few microns can now be achieved; new restraints are put on the remaining design of the other layers of the device. The thickness of the dielectric layer should be minimized while still maintaining low leakage.

E. Conclusion

By replacing a fully printed OTFT-architecture with a laser scribed channel, the channel length could be reduced from 40-50 µm, to 5 µm. A narrow channel could be opened after annealing at 140 ºC however the process resulted in sharp scale formation and could not be implemented in a transistor structure. Laser scribing of a channel on lightly annealed prints followed by a post annealing at 140ºC showed good edge definition without scale formation. The width of the channel could be tuned below the half width of the laser beam and the laser pulse energy could be varied within one order of magnitude without inducing any visible damage in the substrate. Laser channels down to 4-5 µm could be scribed with the developed methodology, with a laser beam diameter of 15-16 µm. The ablation threshold was larger on the lightly annealed films due to remaining residues of solvents absorbing part of the laser energy. The energy profile of the Gaussian beam with energy below the ablation threshold anneals the film resulting in locally increased ablation threshold in this region. This can be seen as a laser annealed line rather than an opened line if successive pulses overlap with the annealed region from the previous pulse rather than a fresh area, this occur at very slow processing speeds and pulse energy just above the ablation threshold. The ablation threshold was independent of the wavelength with a fluence threshold of 0.10 µJ/cm^2 for the lightly annealed film and 0.040 µJ/cm^2 for the fully annealed film.

ACKNOWLEDGMENTS

The authors would like to thank Thin Film Electronics ASA for close collaboration and financing of this research together with the Norwegian Research Council under project number 235386.

REFERENCES

1 Y. Takeda, K. Hayasaka, R. Shiwaku, K. Yokosawa, T. Shiba, M. Mamada, D. Kumaki, K. Fukuda, and S. Tokito, Scientific Reports **6,** 25714 (2016).
2 J. Noh, M. Jung, Y. Jung, C. Yeom, M. Pyo, and G. Cho, Proceedings of the IEEE **103,** 554 (2015).
3 M. Saumen and N. Yong-Young, Semiconductor Science and Technology **30,** 064003 (2015).
4 H. Lee, D. Lee, J. Hwang, D. Nam, C. Byeon, S. H. Ko, and S. Lee, Optics Express **22,** 8919 (2014).
5 S. G. Bucella, G. Nava, K. C. Vishunubhatla, and M. Caironi, Organic Electronics **14,** 2249 (2013).
6 S. H. Ko, H. Pan, C. P. Grigoropoulos, J. M. J. Fréchet, C. K. Luscombe, and D. Poulikakos, Applied Physics A **92,** 579 (2008).
7 S. S. Harilal, *Laser-Induced Breakdown Spectroscopy*, Vol. 182 (Springer-Verlag Berlin Heidelberg, 2014).
8 J. M. Liu, Opt. Lett. **7,** 196 (1982).
9 J. Bonse, J. M. Wrobel, J. Krüger, and W. Kautek, Applied Physics A **72,** 89 (2001).
10 S. H. Ko, H. Pan, D. J. Hwang, J. Chung, S. Ryu, C. P. Grigoropoulos, and D. Poulikakos, Journal of Applied Physics **102,** 093102 (2007).
11 A. Chiolerio, G. Maccioni, P. Martino, M. Cotto, P. Pandolfi, P. Rivolo, S. Ferrero, and L. Scaltrito, Microelectronic Engineering **88,** 2481 (2011).
12 T. Kumpulainen, J. Pekkanen, J. Valkama, J. Laakso, R. Tuokko, and M. Mäntysalo, Optics & Laser Technology **43,** 570 (2011).
13 L. Gallais, E. Bergeret, B. Wang, M. Guerin, and E. Bènevent, Applied Physics A**,** 1 (2013).
14 D. Bauerle, *Laser Processing and Chemistry*, 3rd ed. (Springer, 2011).
15 L. Gallais, E. Bergeret, B. Wang, M. Guerin, and E. Bènevent, Applied Physics A **115,** 177 (2014).

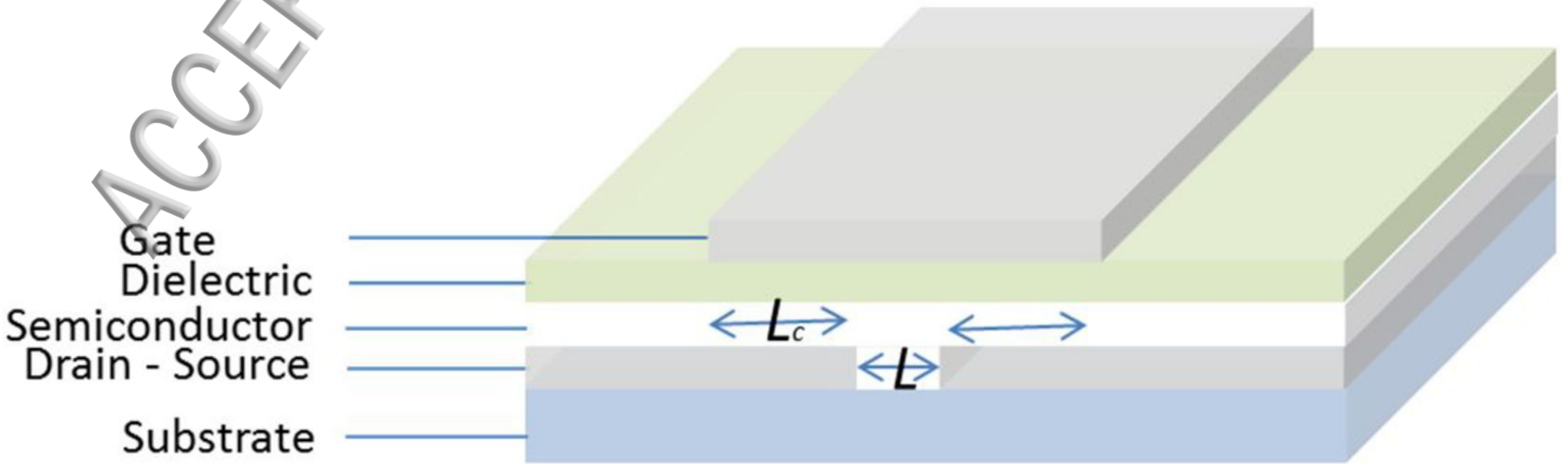
Gate
Dielectric
Semiconductor
Drain - Source
Substrate
L_c
L

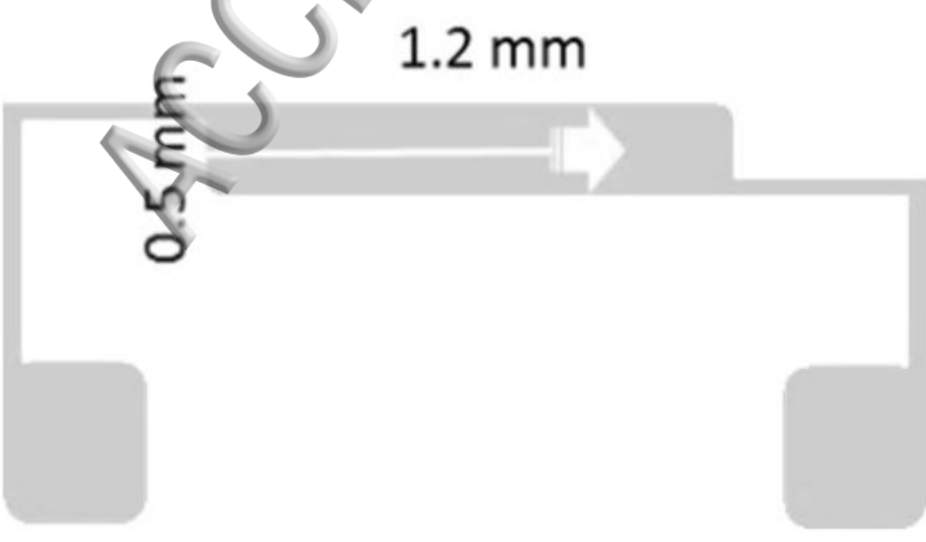
1.2 mm
0.5mm

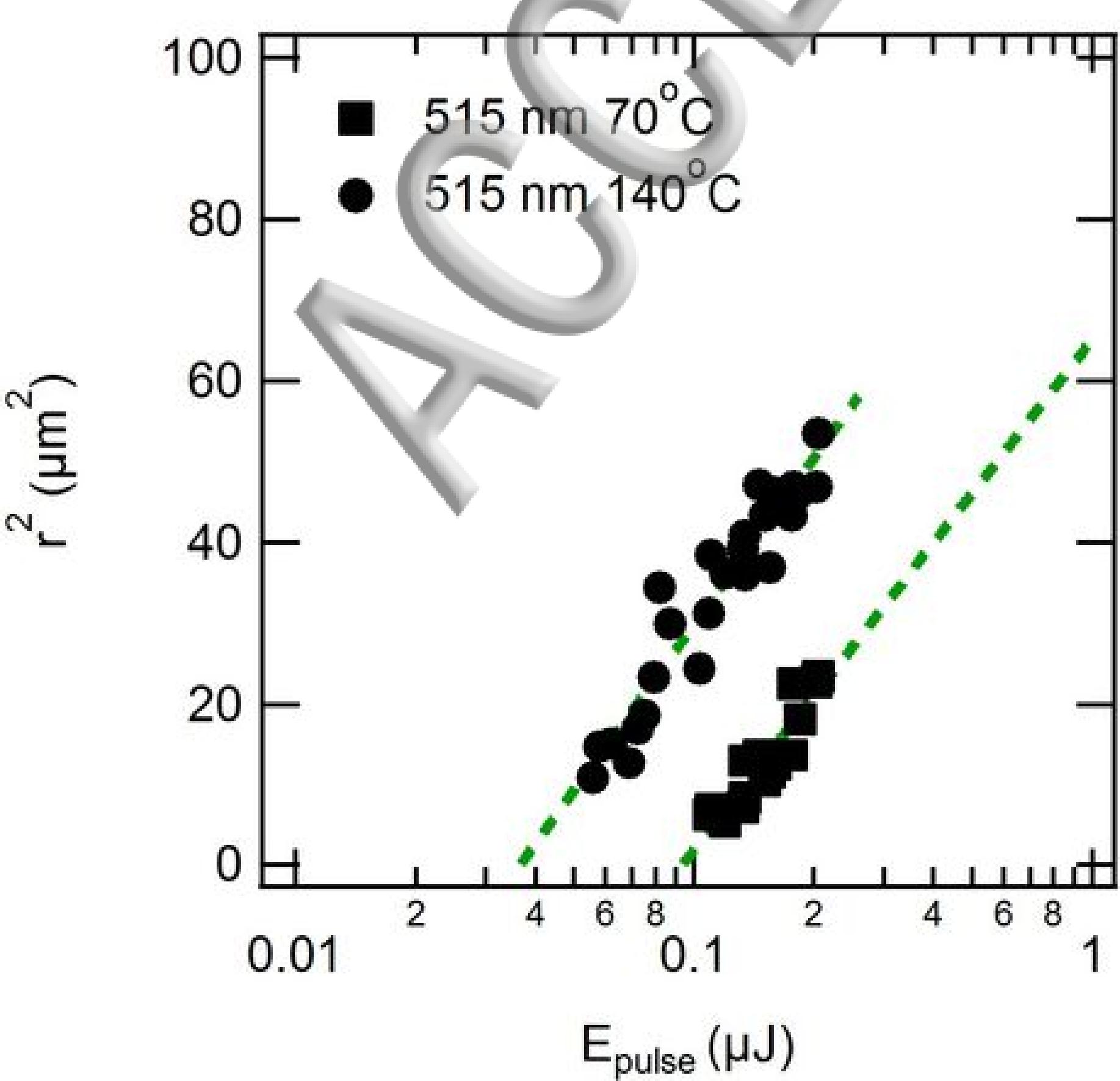
515 nm 70°C
515 nm 140°C
100
80
60
40
20
0
r^2 (μm^2)
0.01
0.1
1
2
4
6
8
E_{pulse} (μJ)

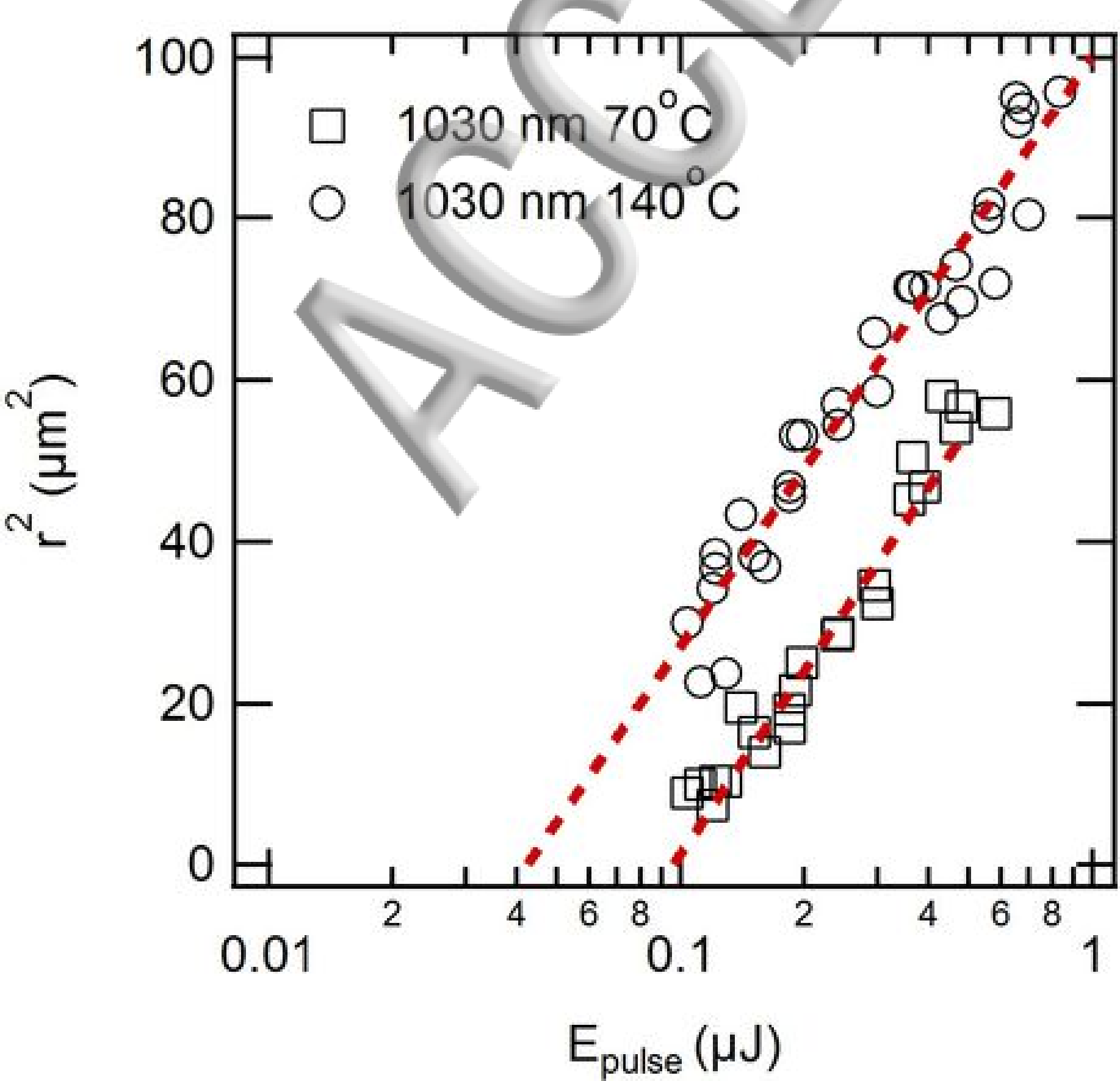
100
80
60
40
20
0
r^2 (μm^2)
1030 nm 70°C
1030 nm 140°C
0.01
2
4
6
8
0.1
2
4
6
8
1
E_{pulse} (μJ)

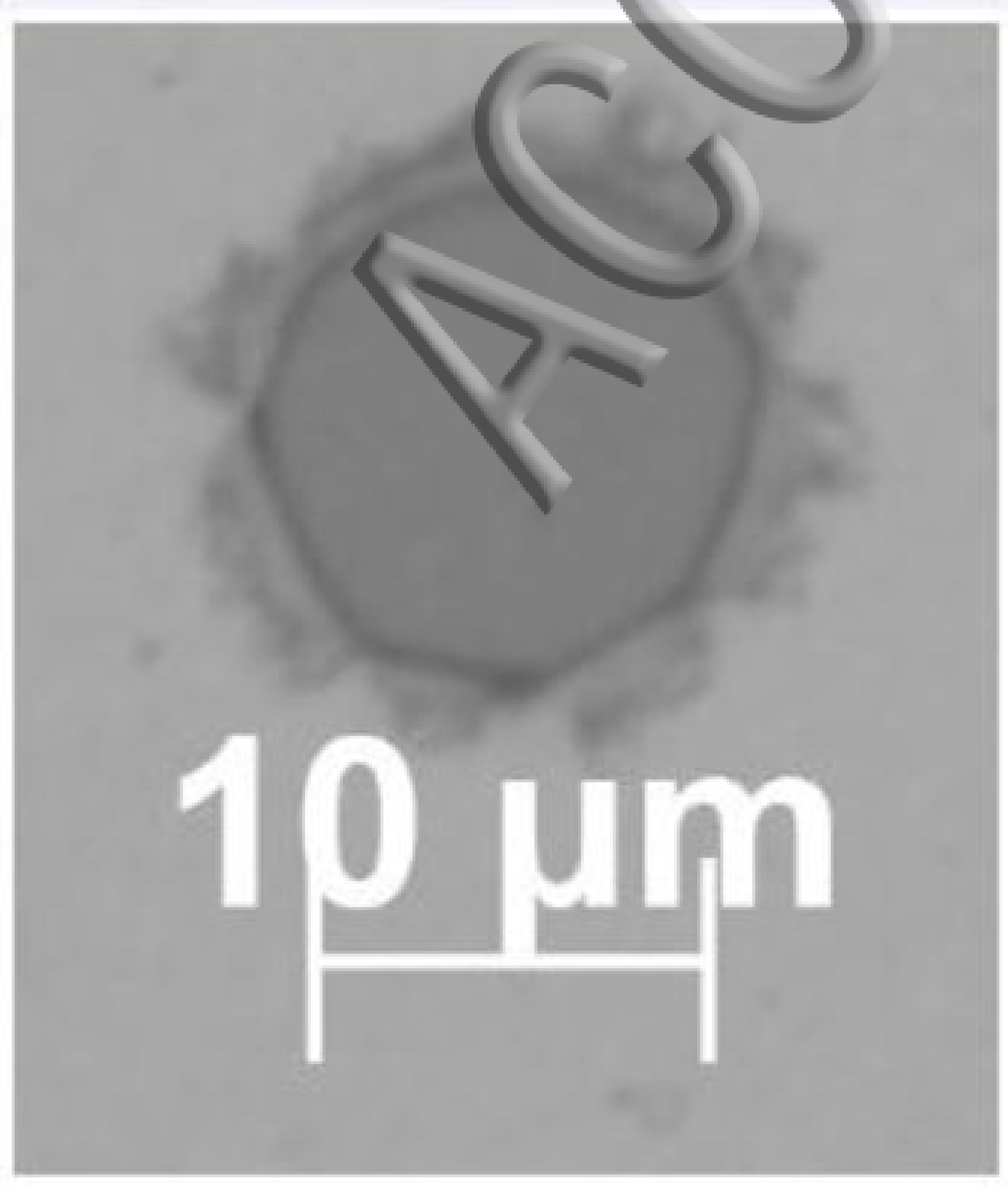
10 µm

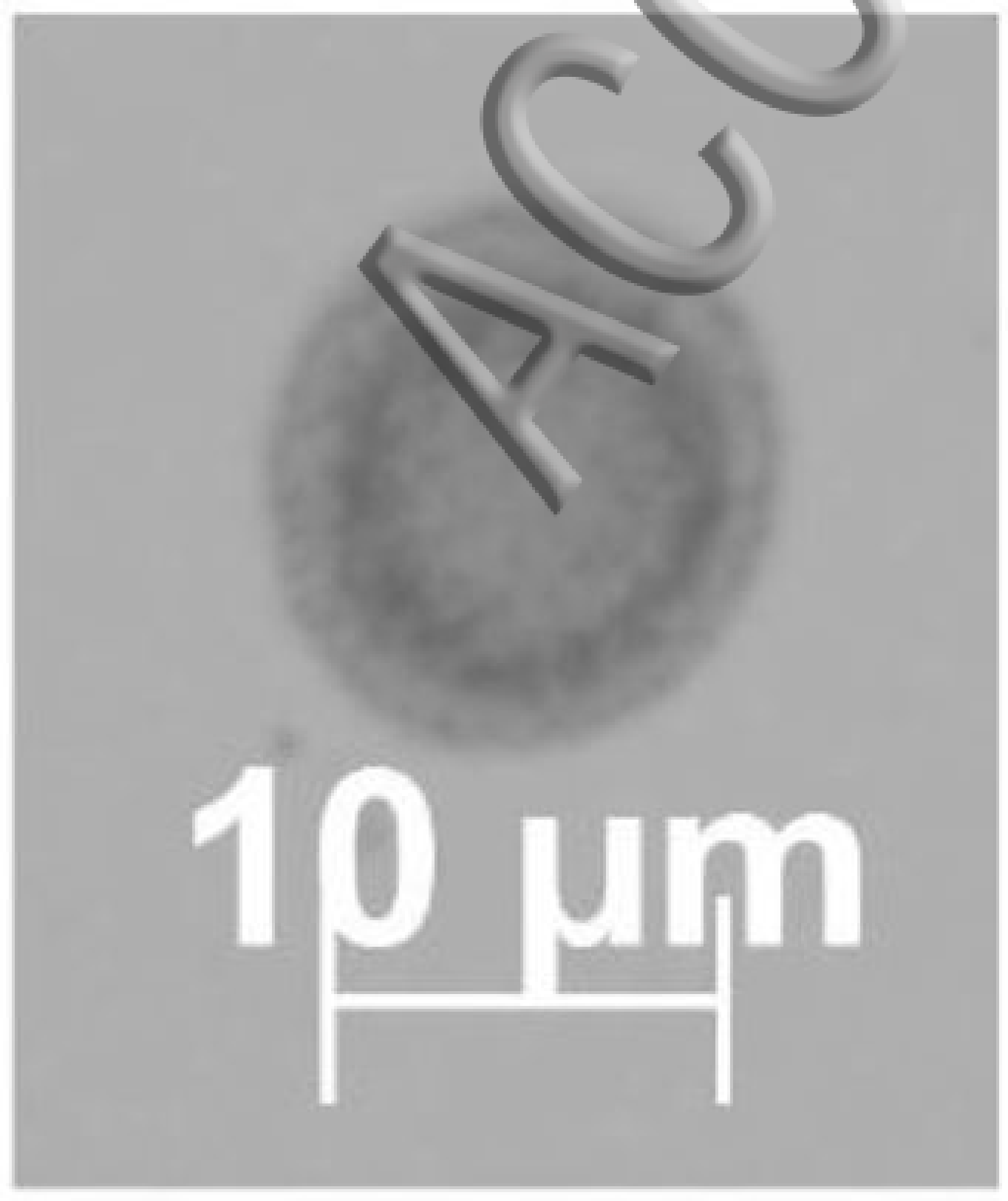
10 µm

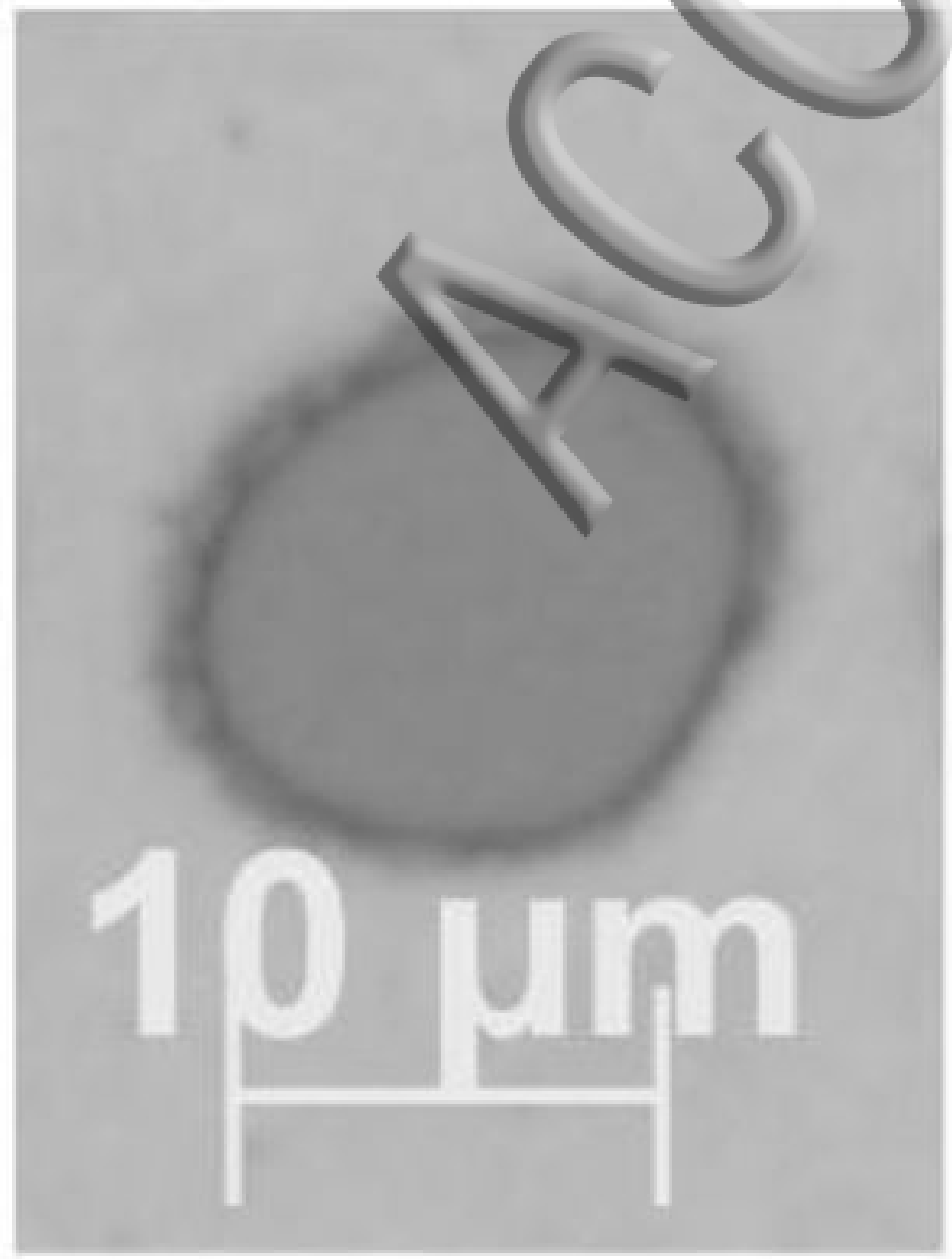
10 µm

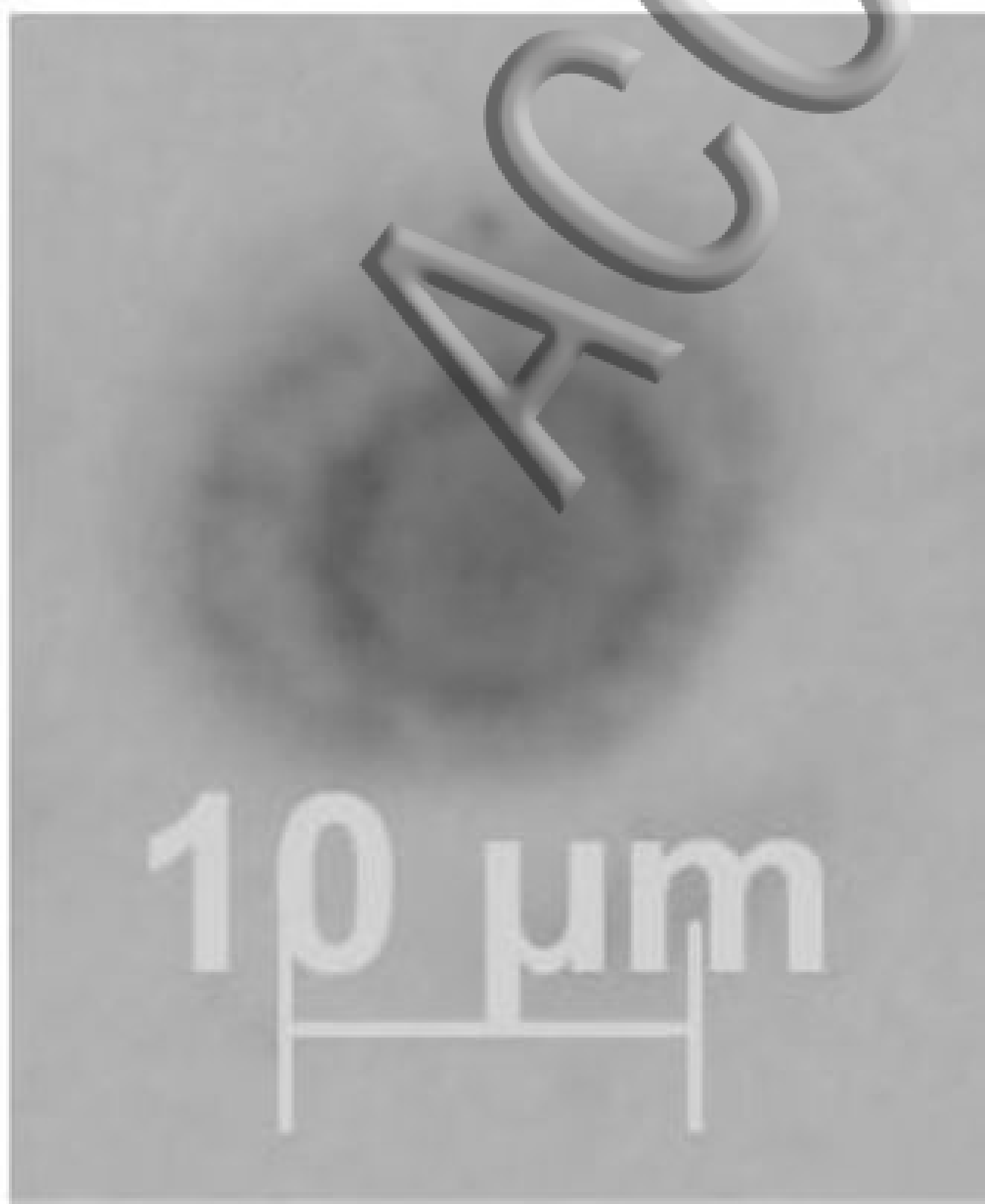
10 µm

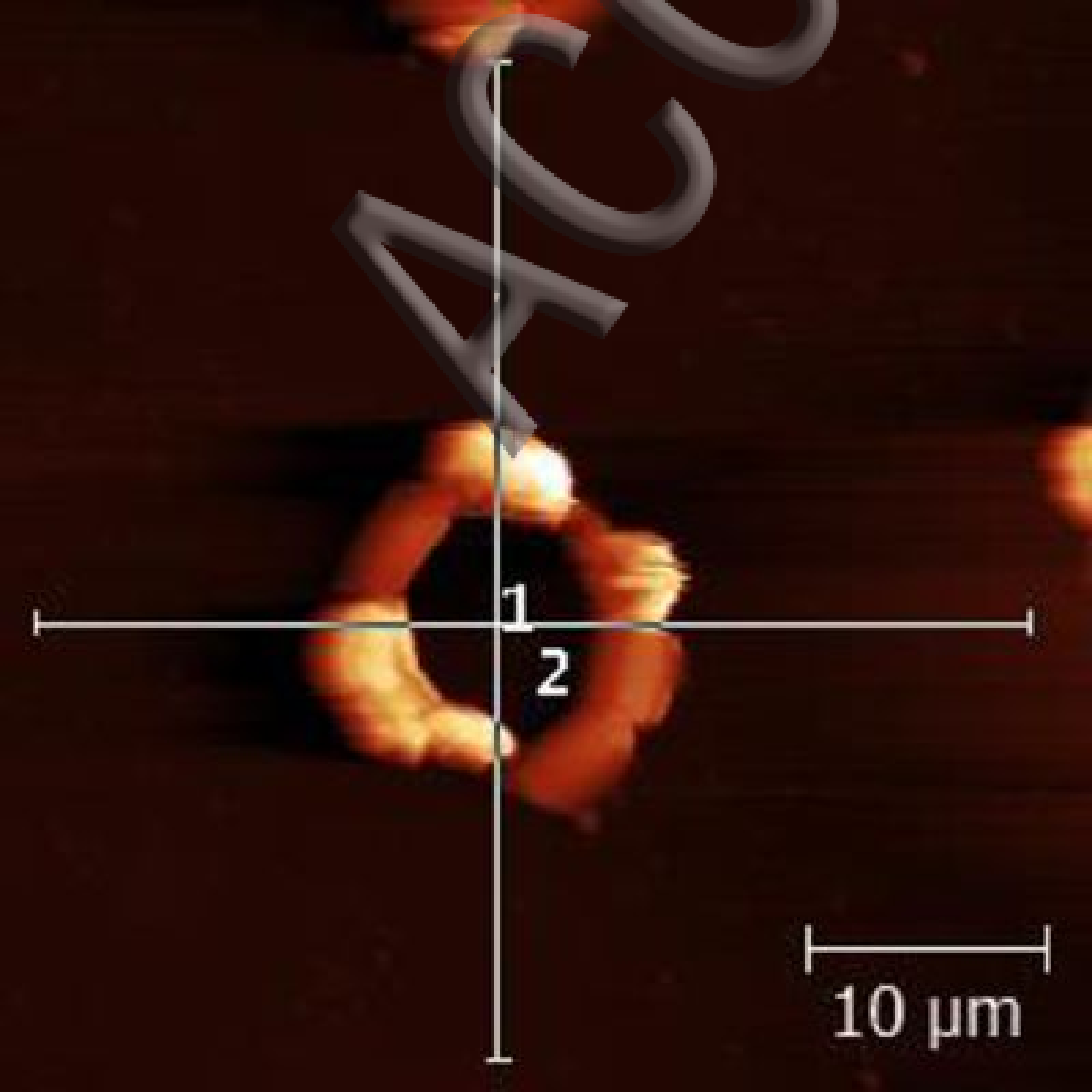
1
2
10 µm

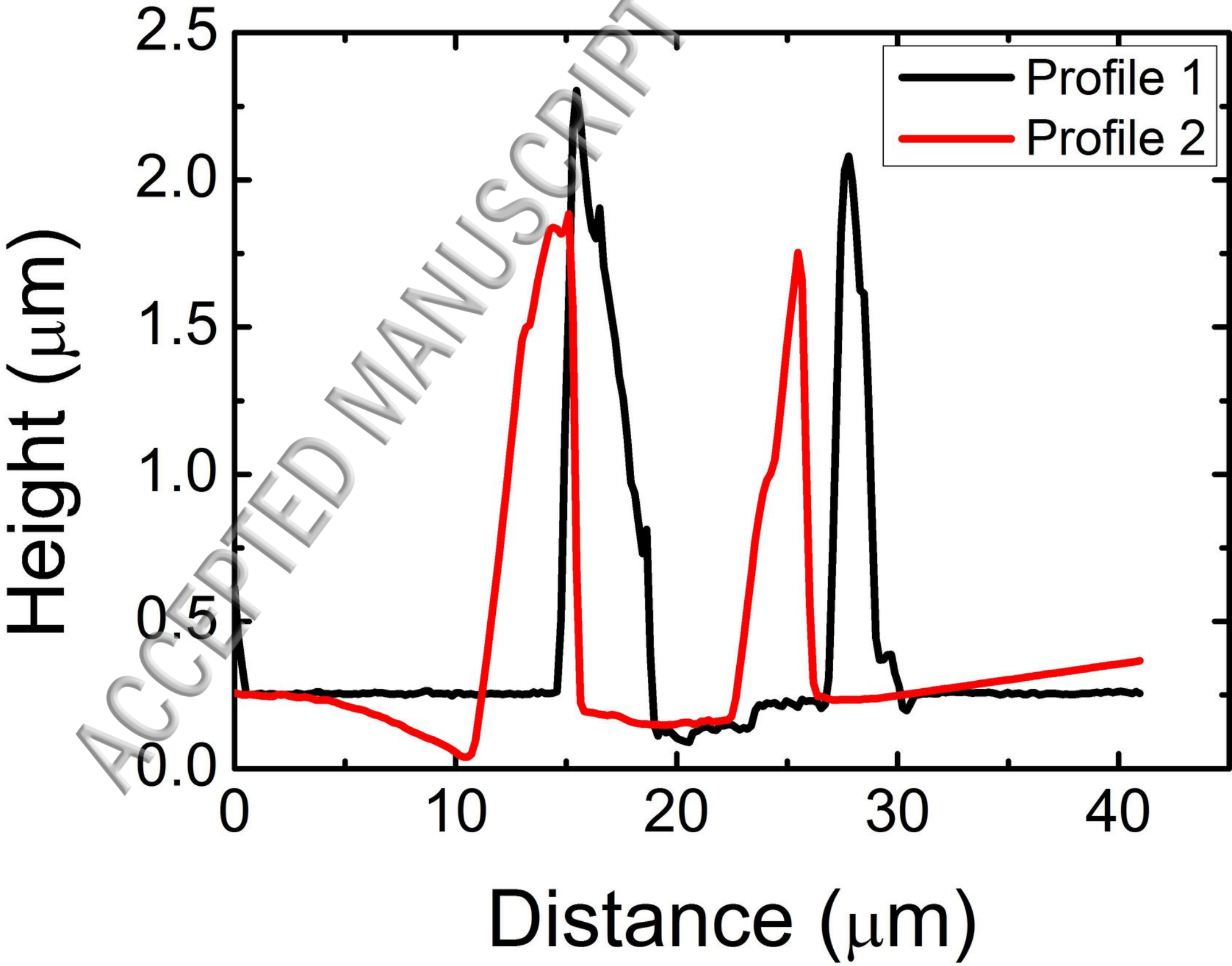

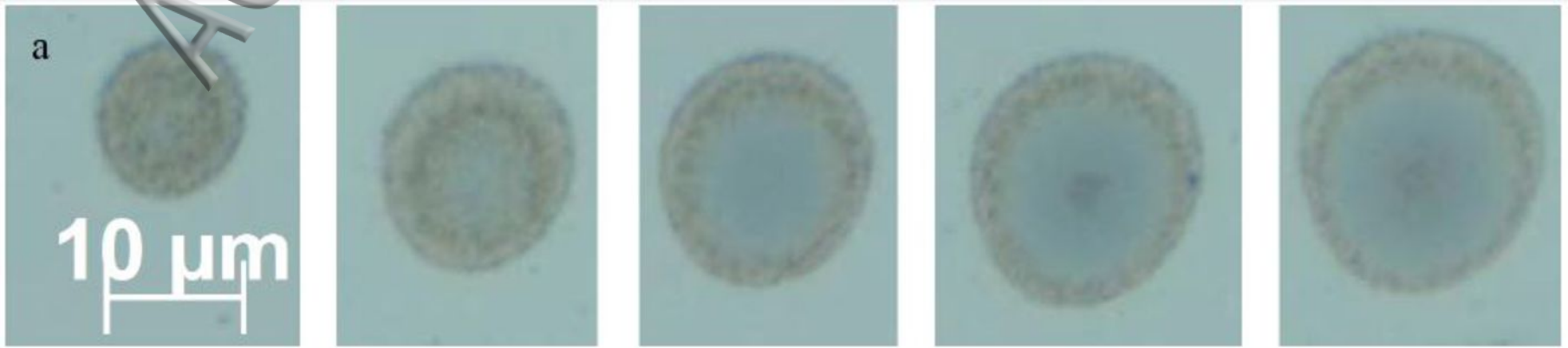
a
10 µm

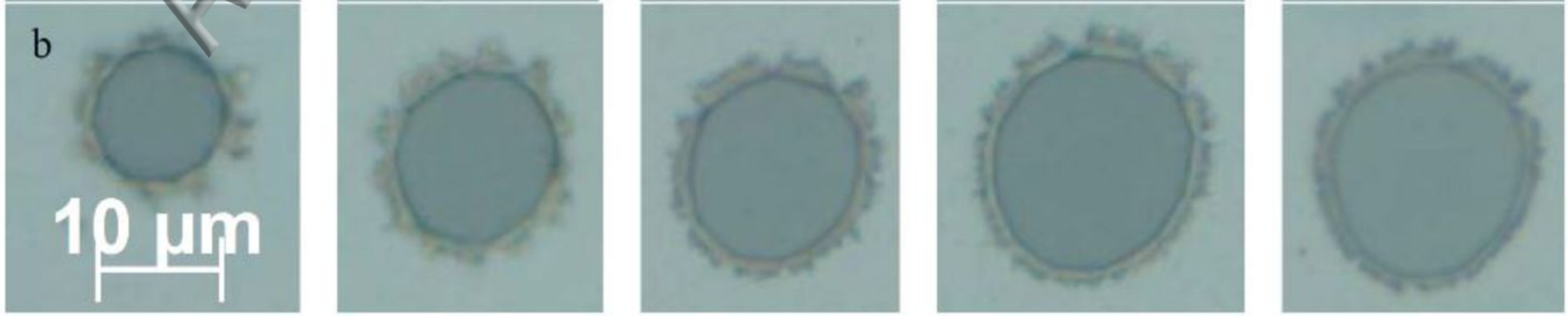
b
10 µm

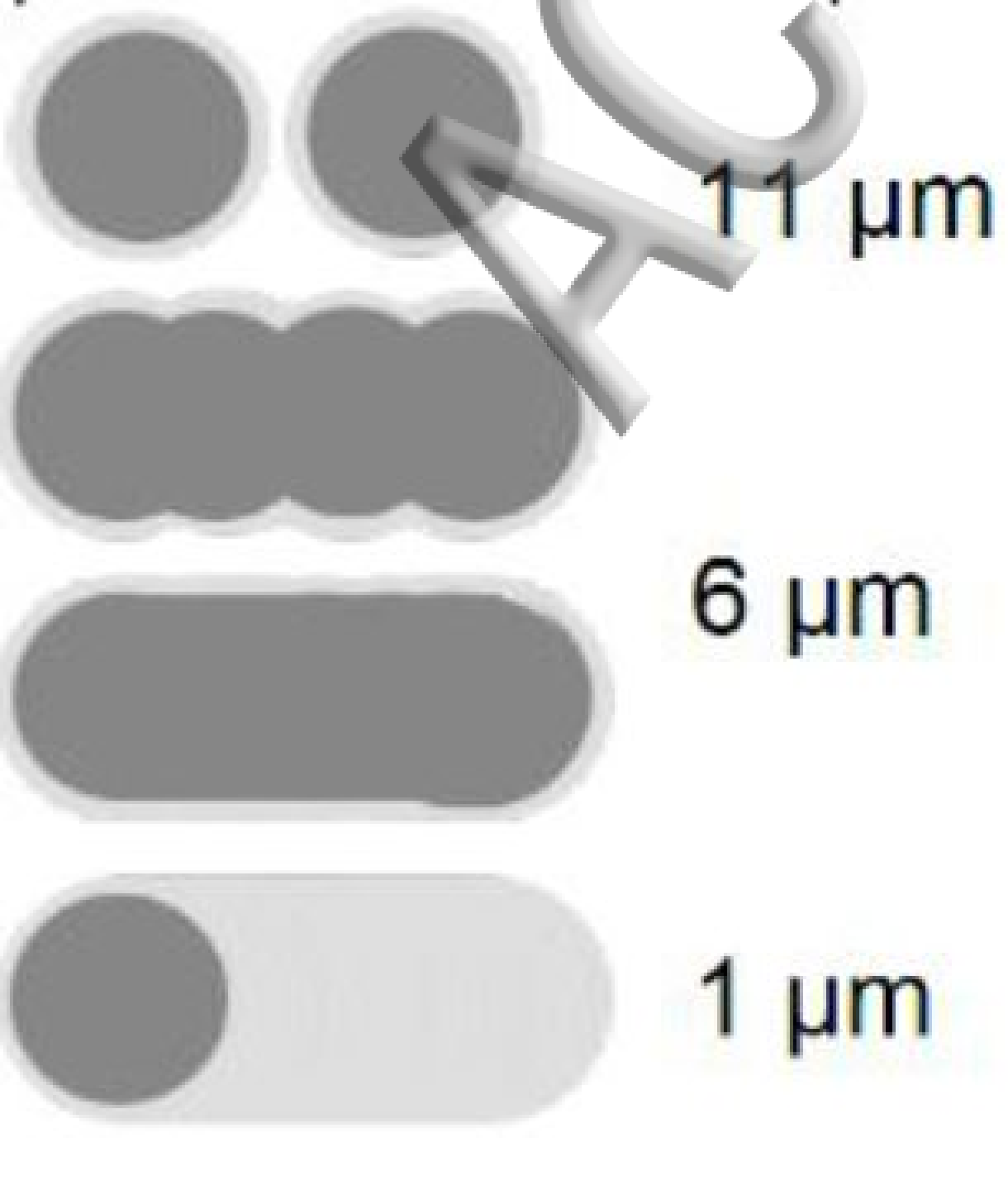
11 µm
6 µm
1 µm

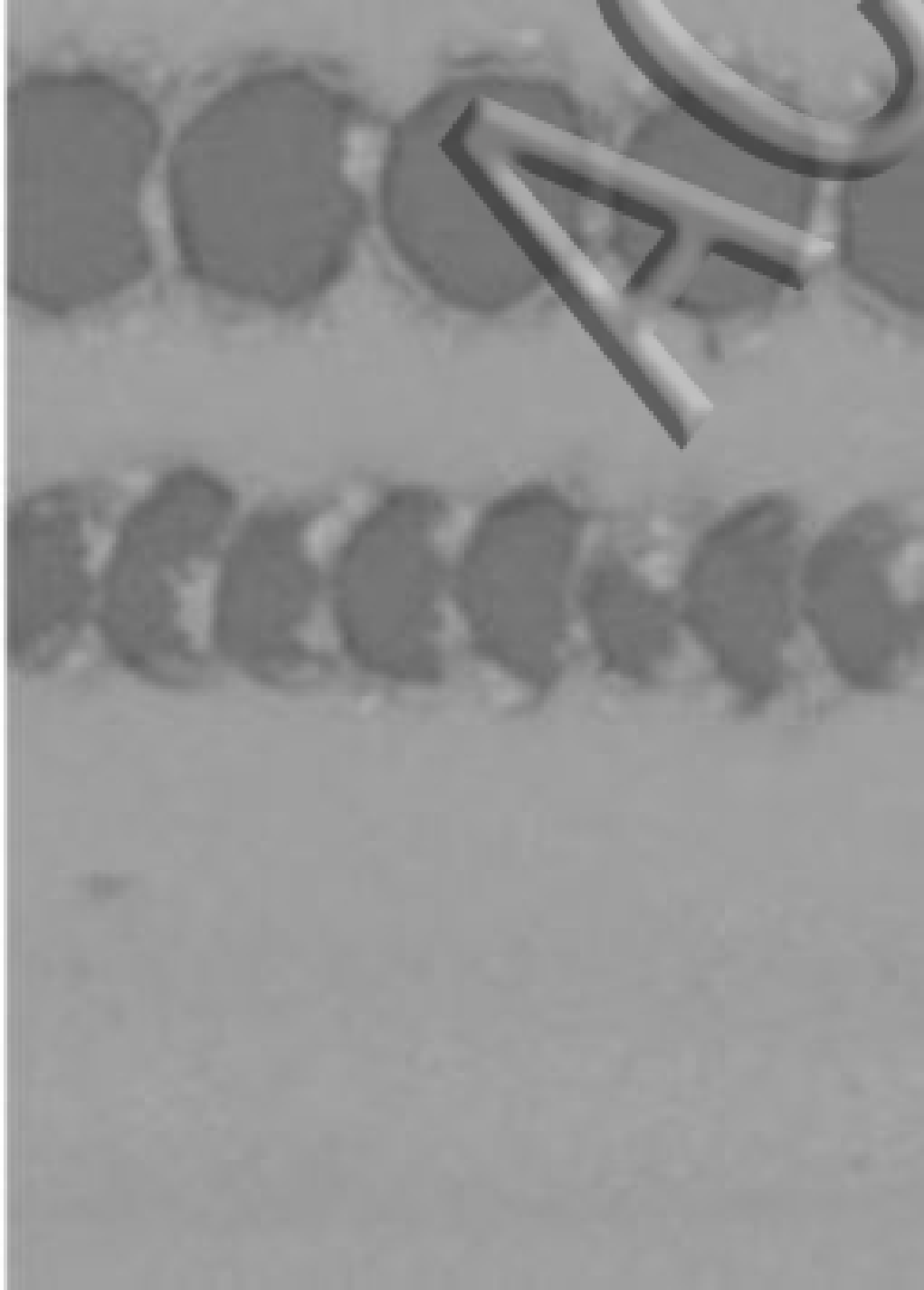

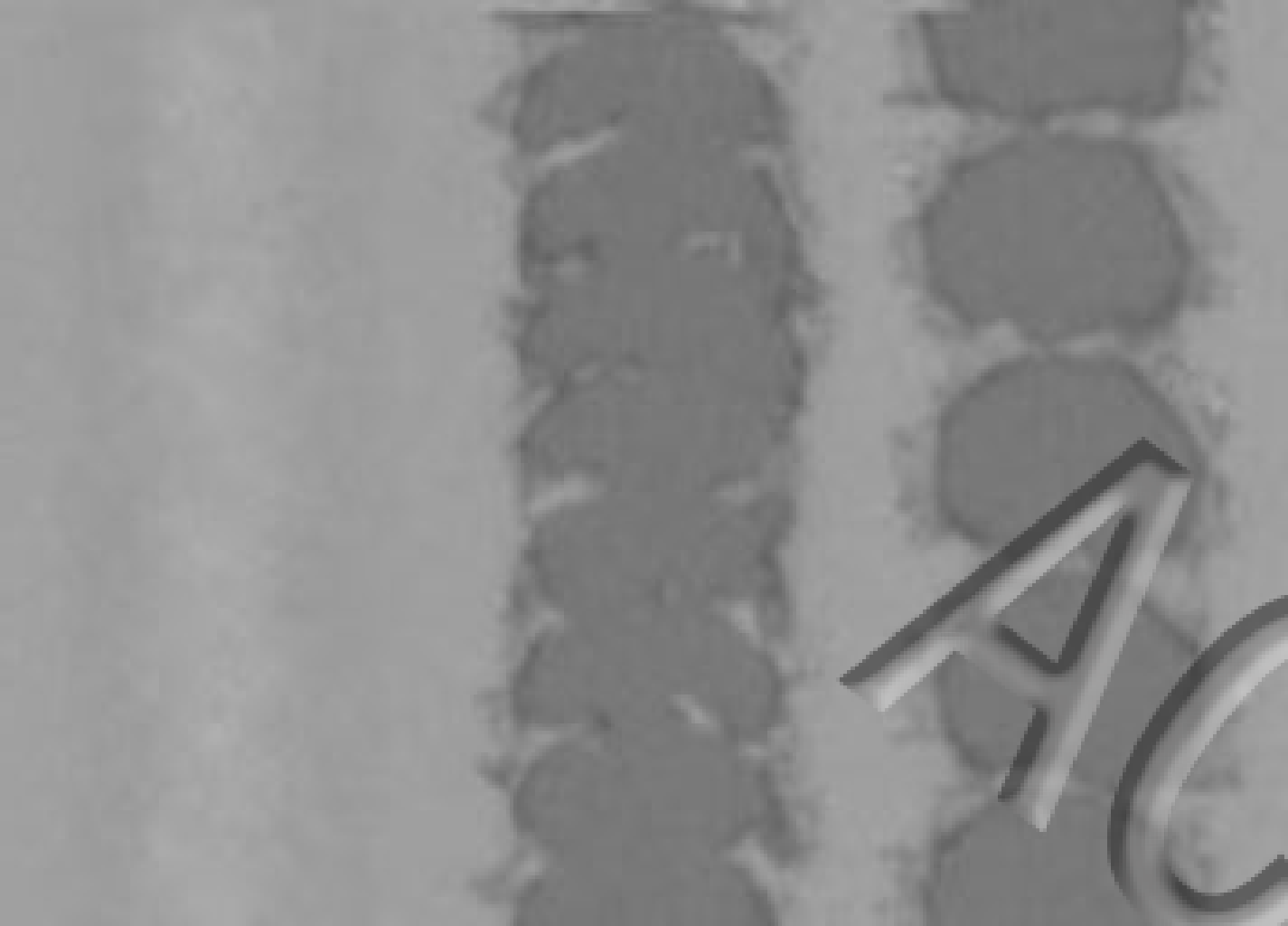

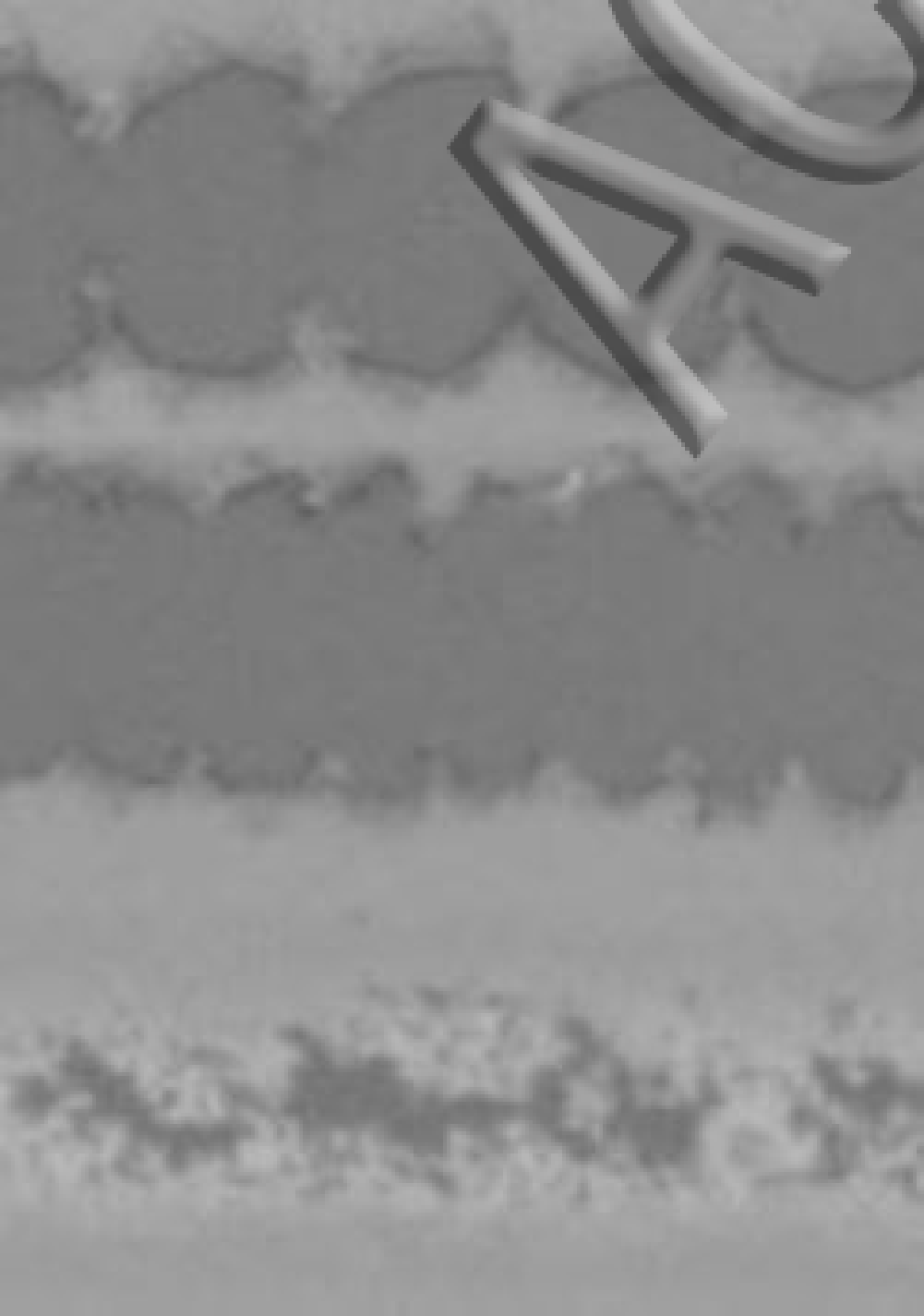

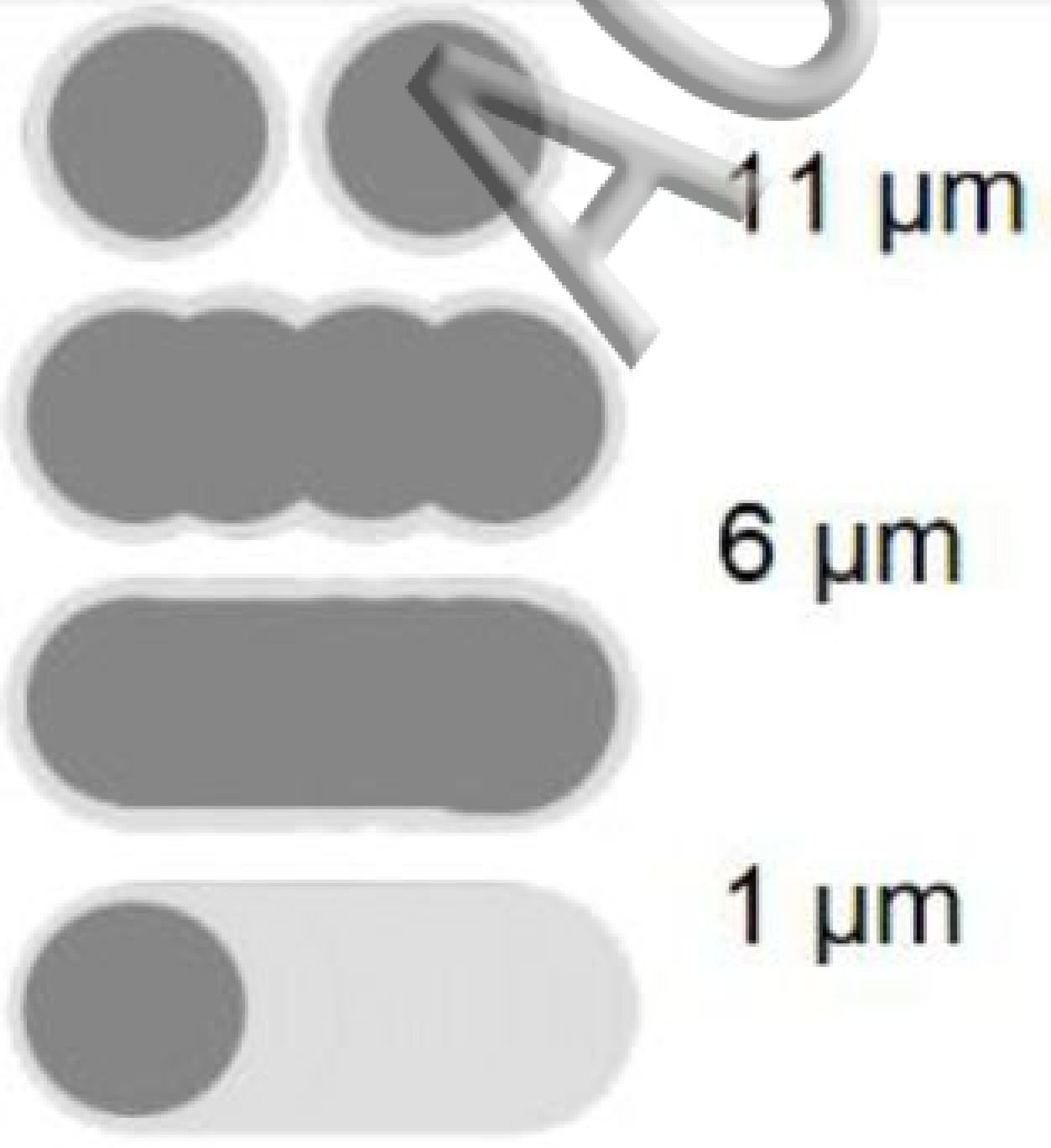
11 µm
6 µm
1 µm

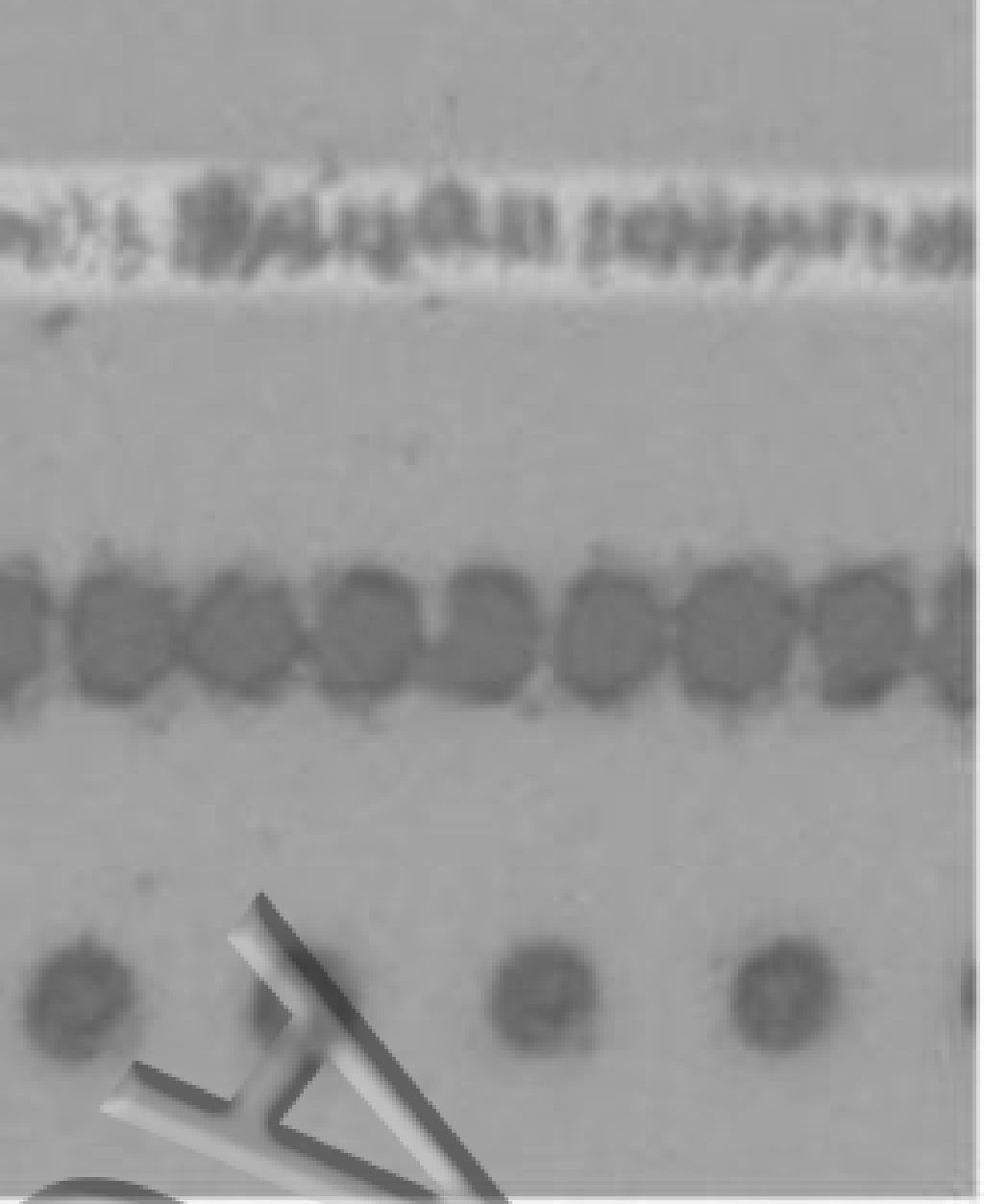

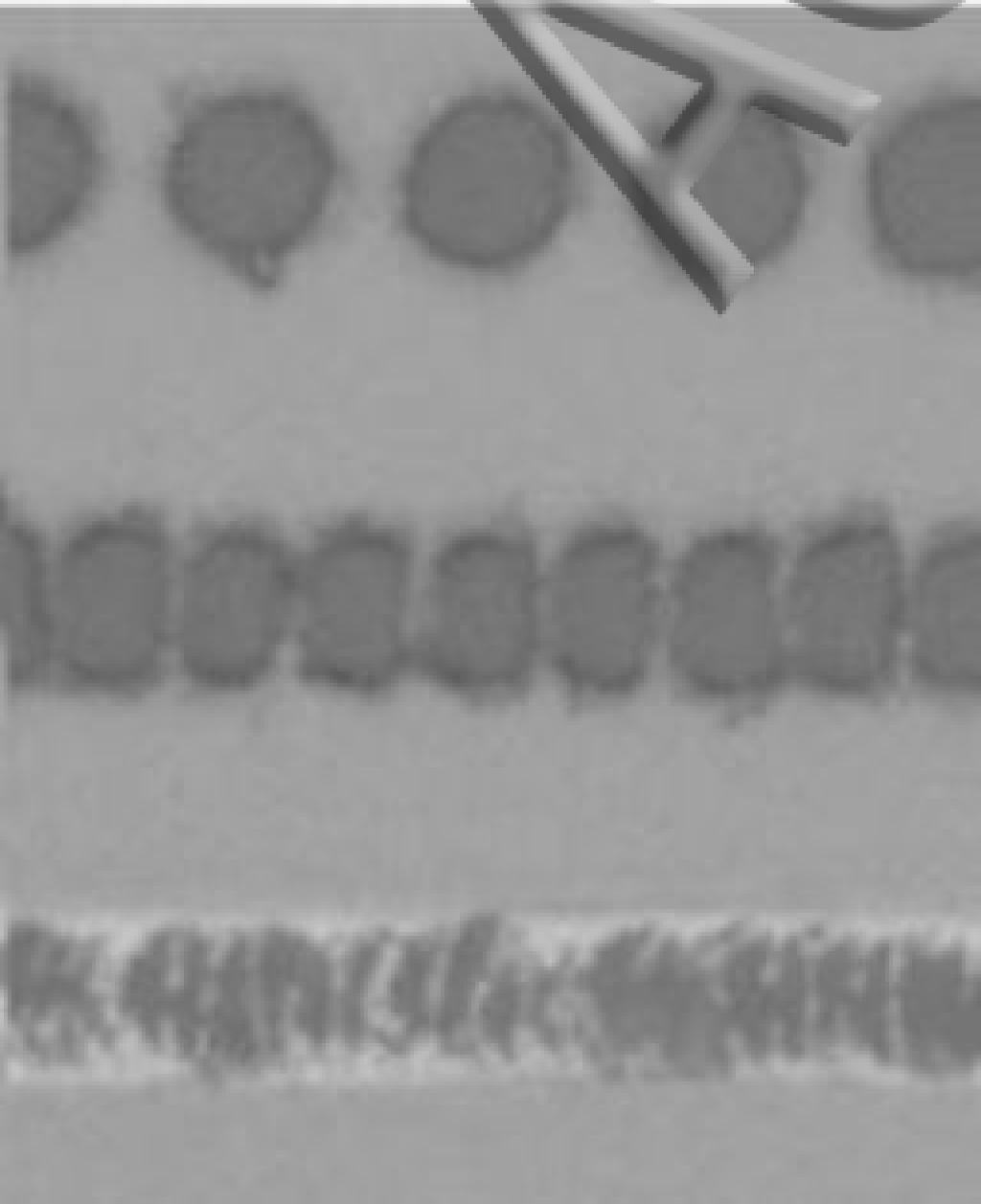

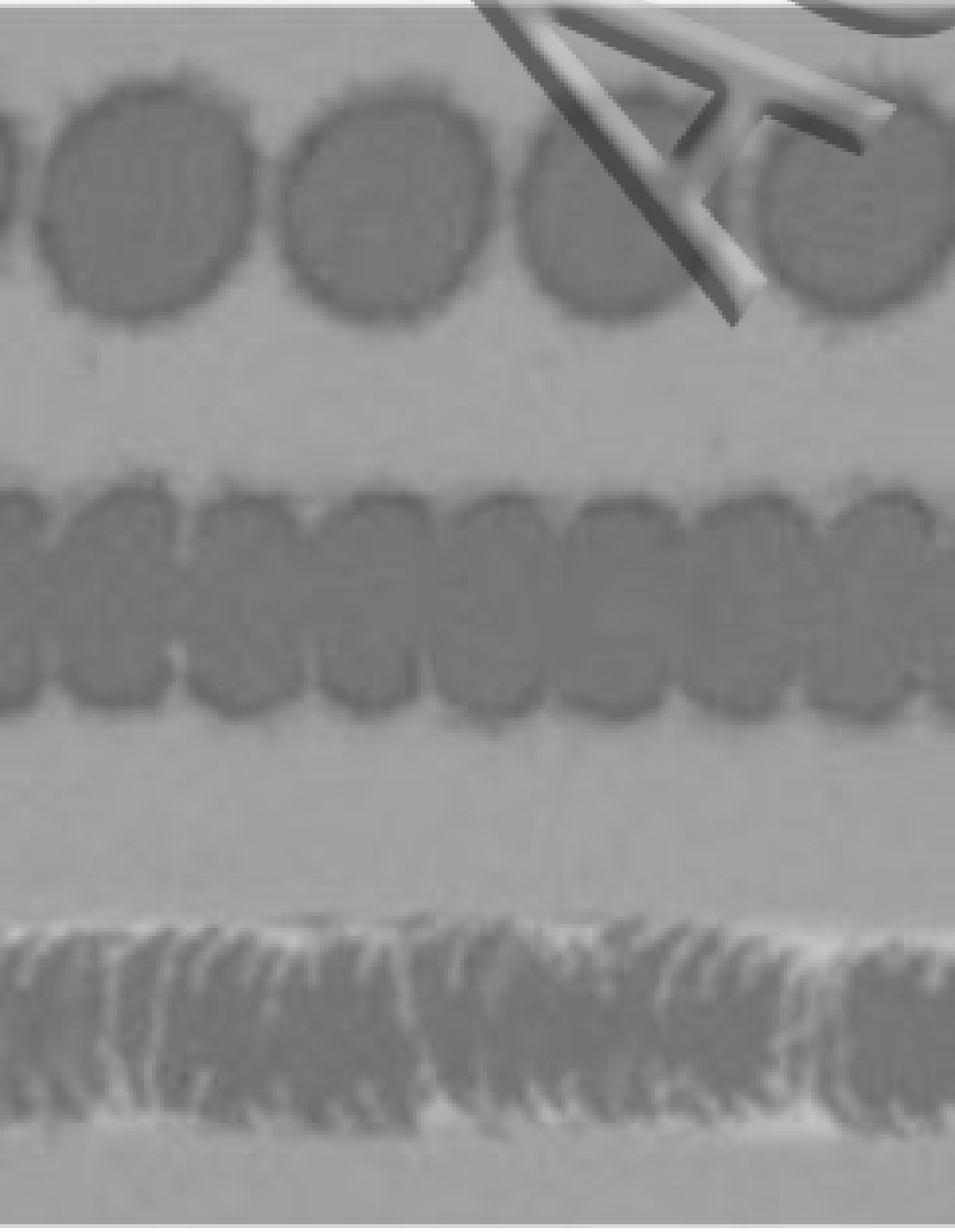

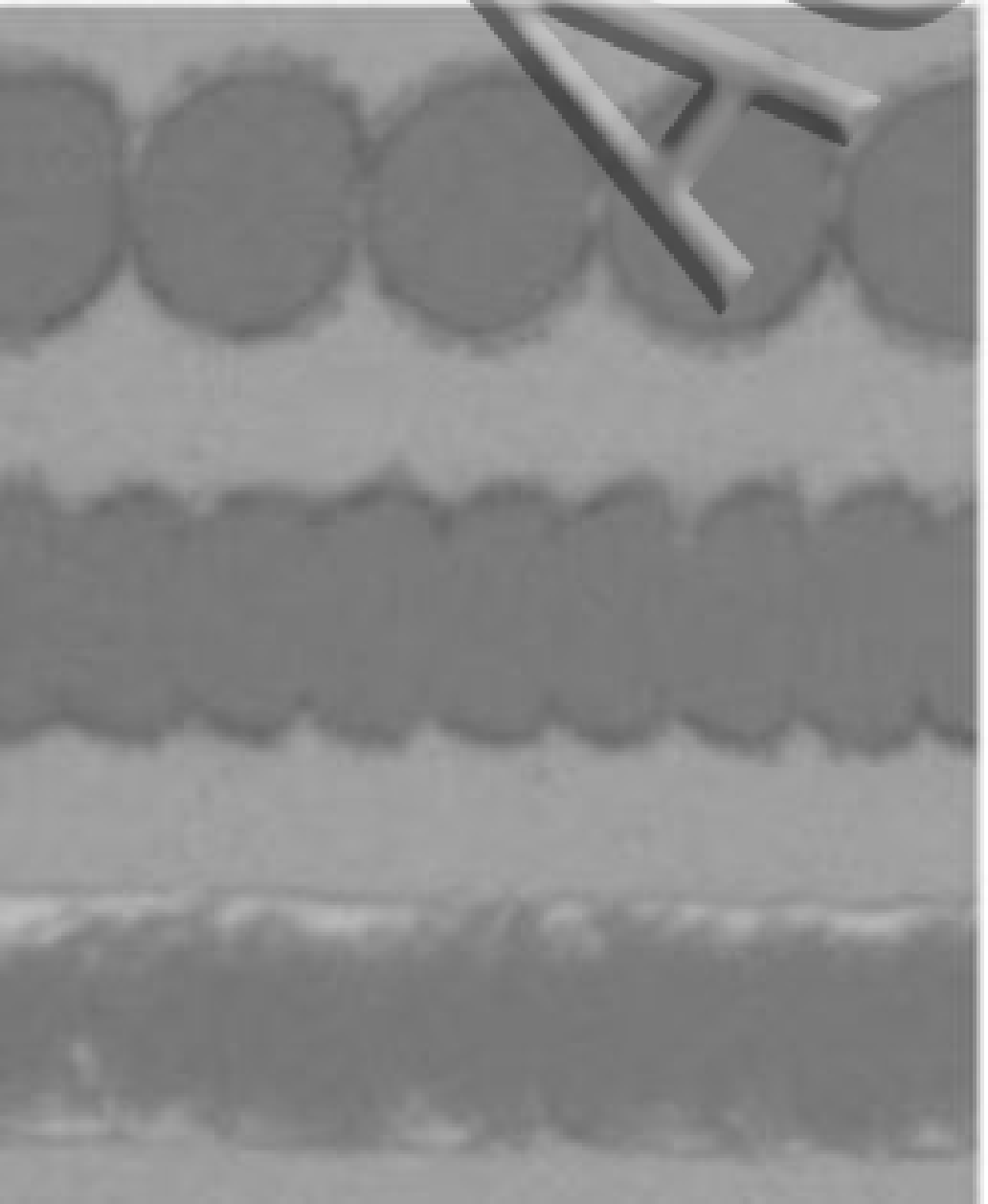

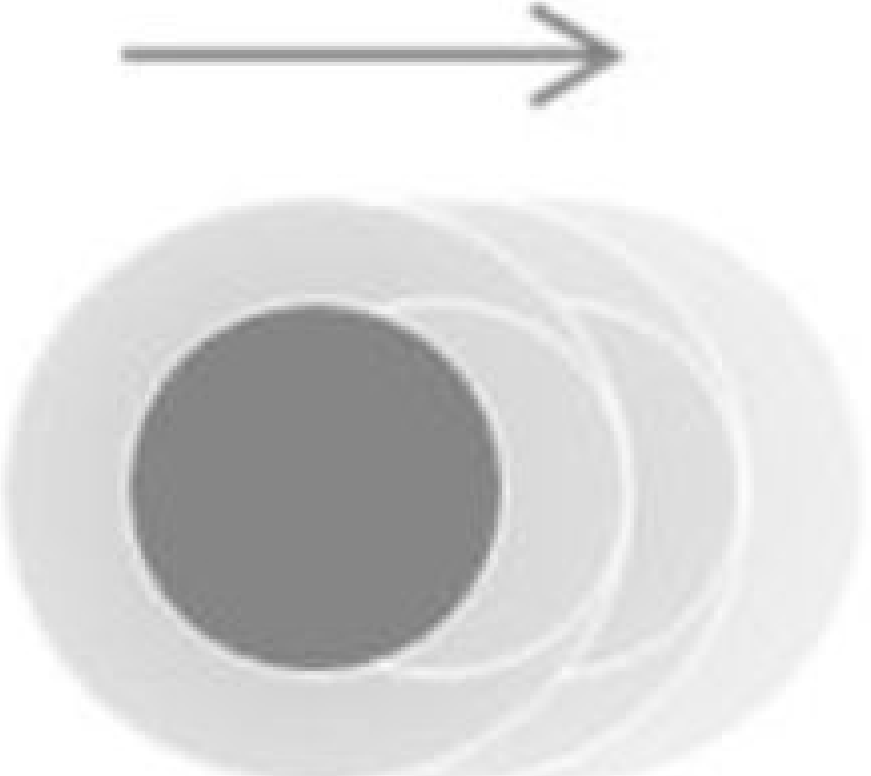

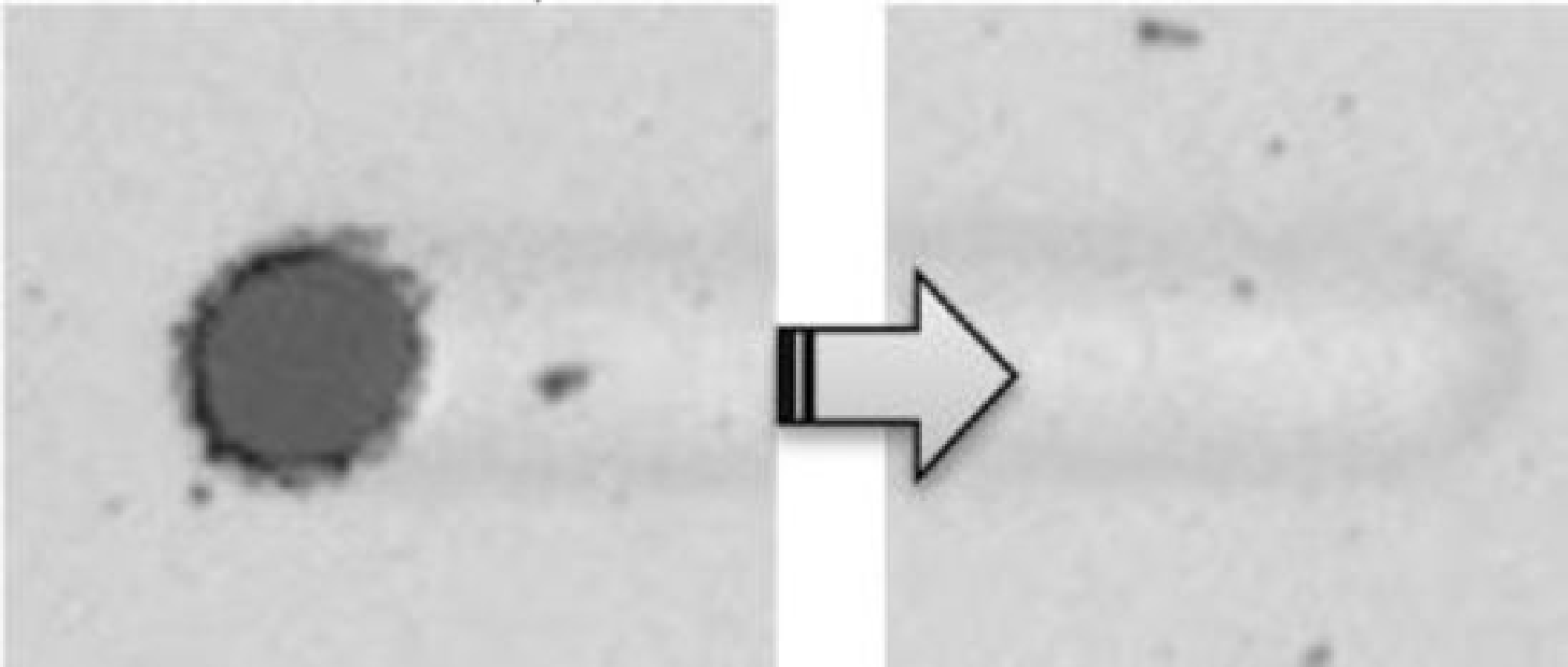

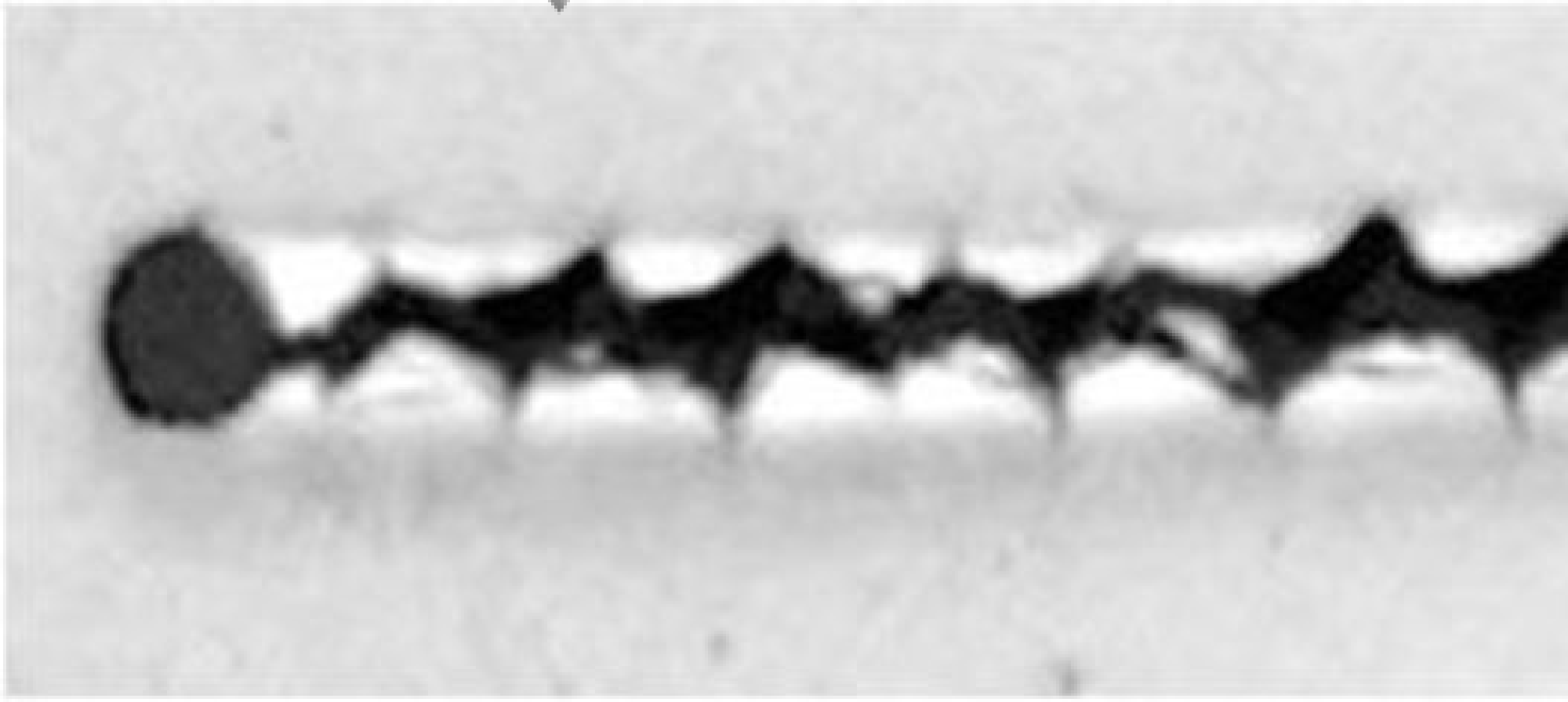

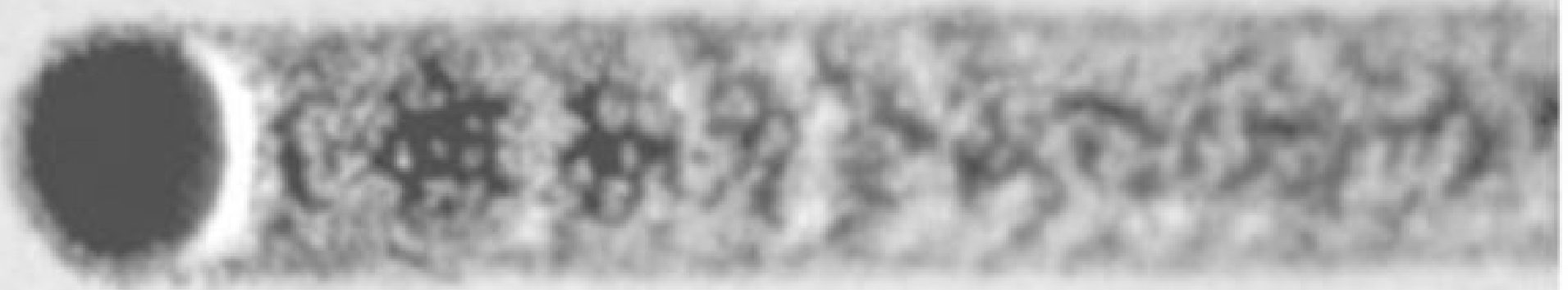

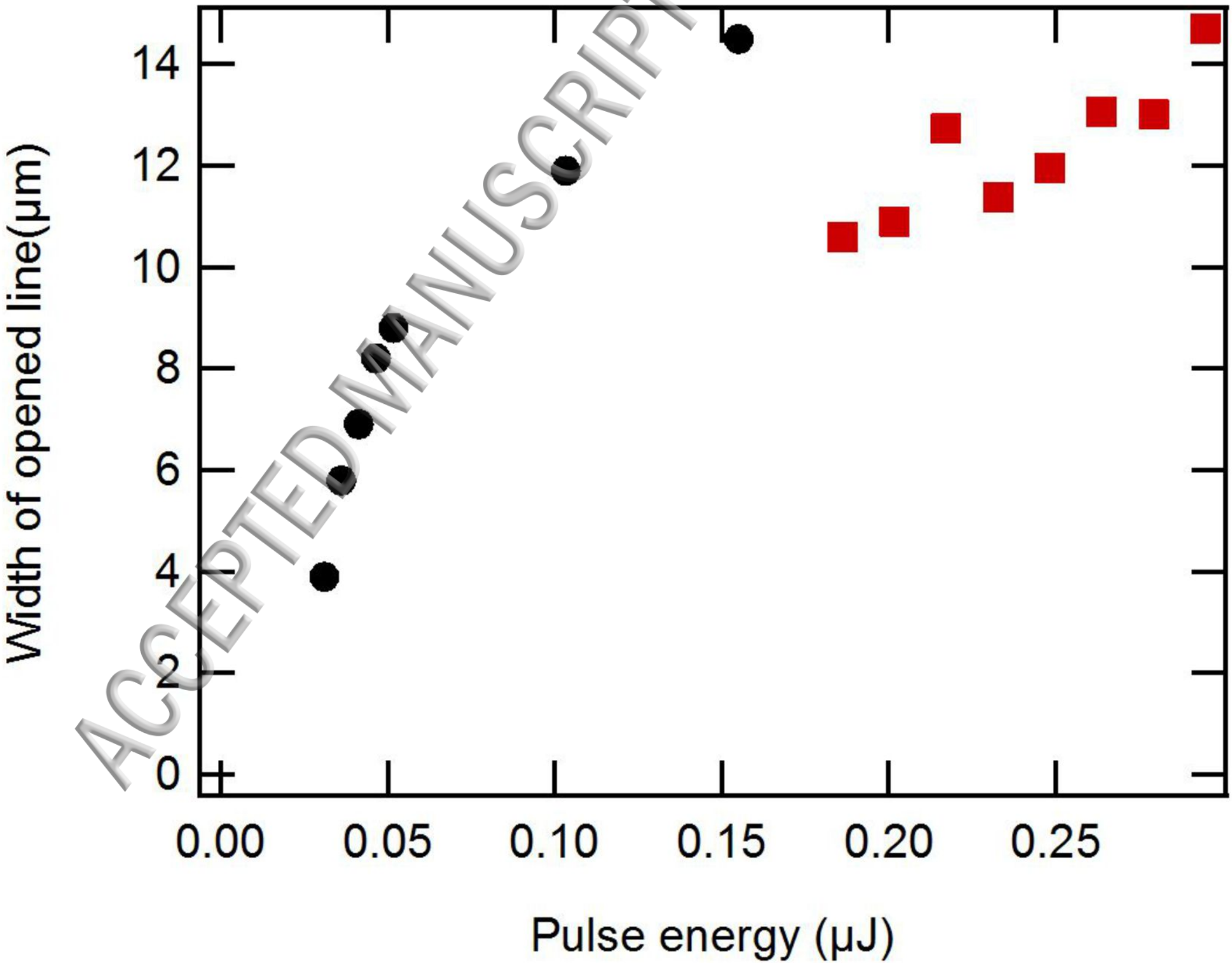

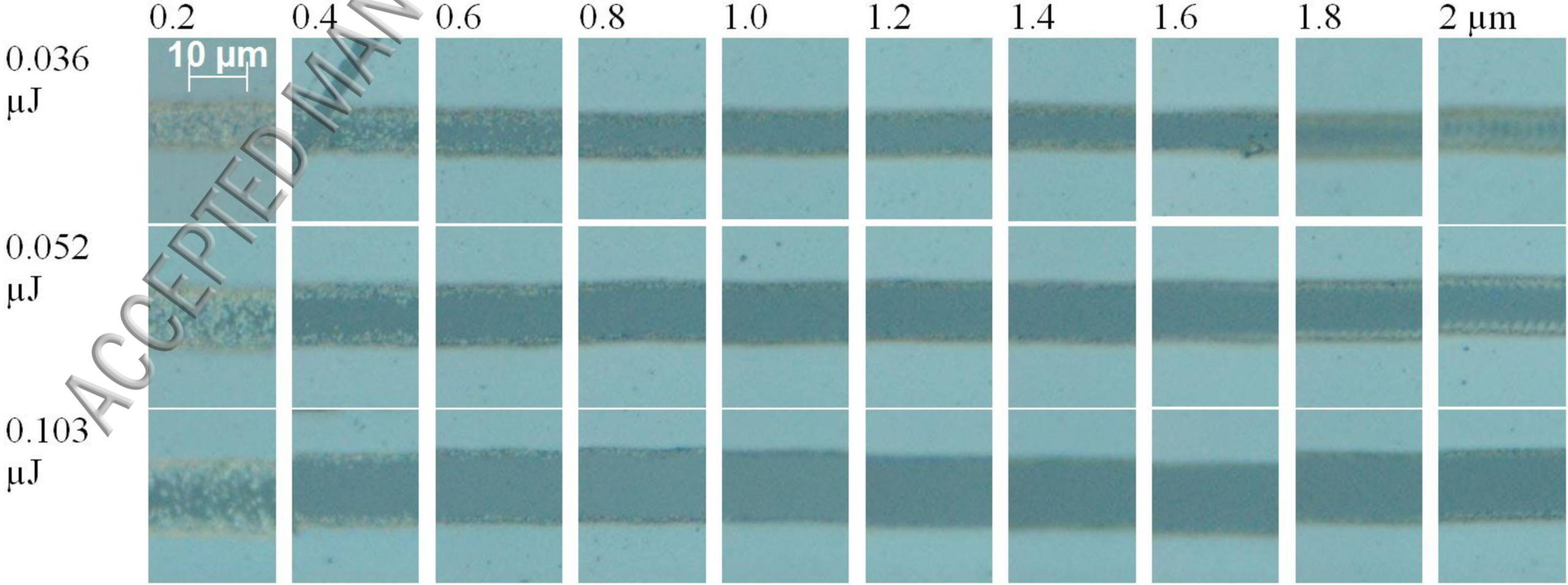

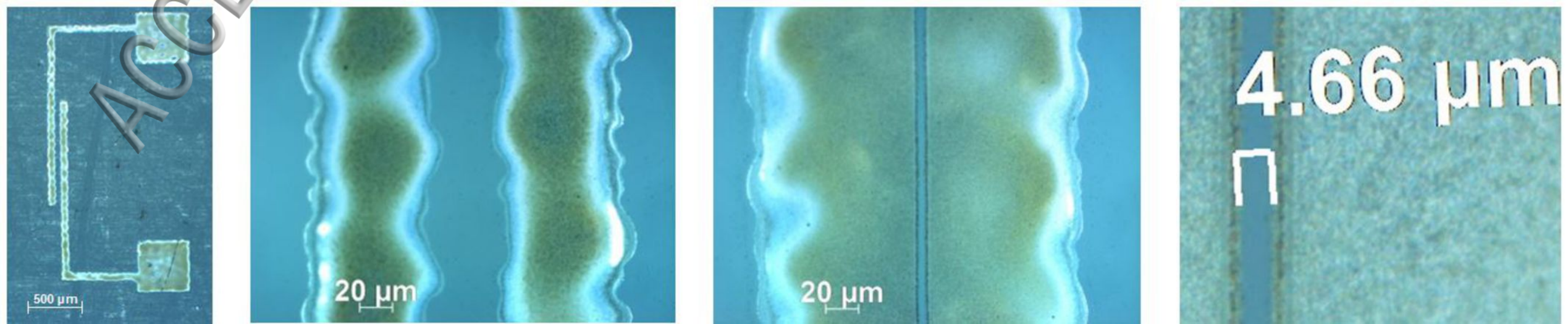
500 µm
20 µm
20 µm
4.66 µm


500 µm

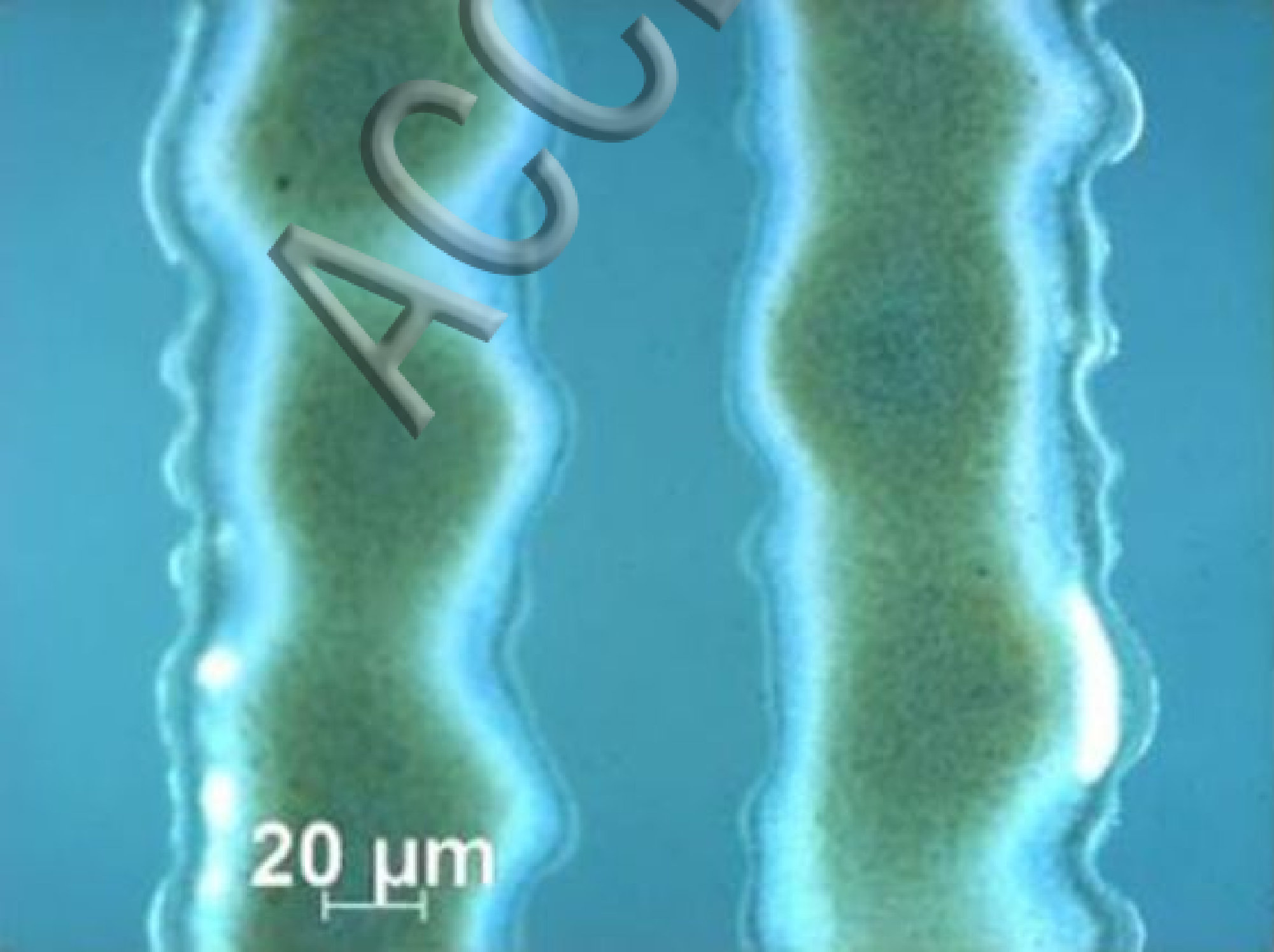
20 µm

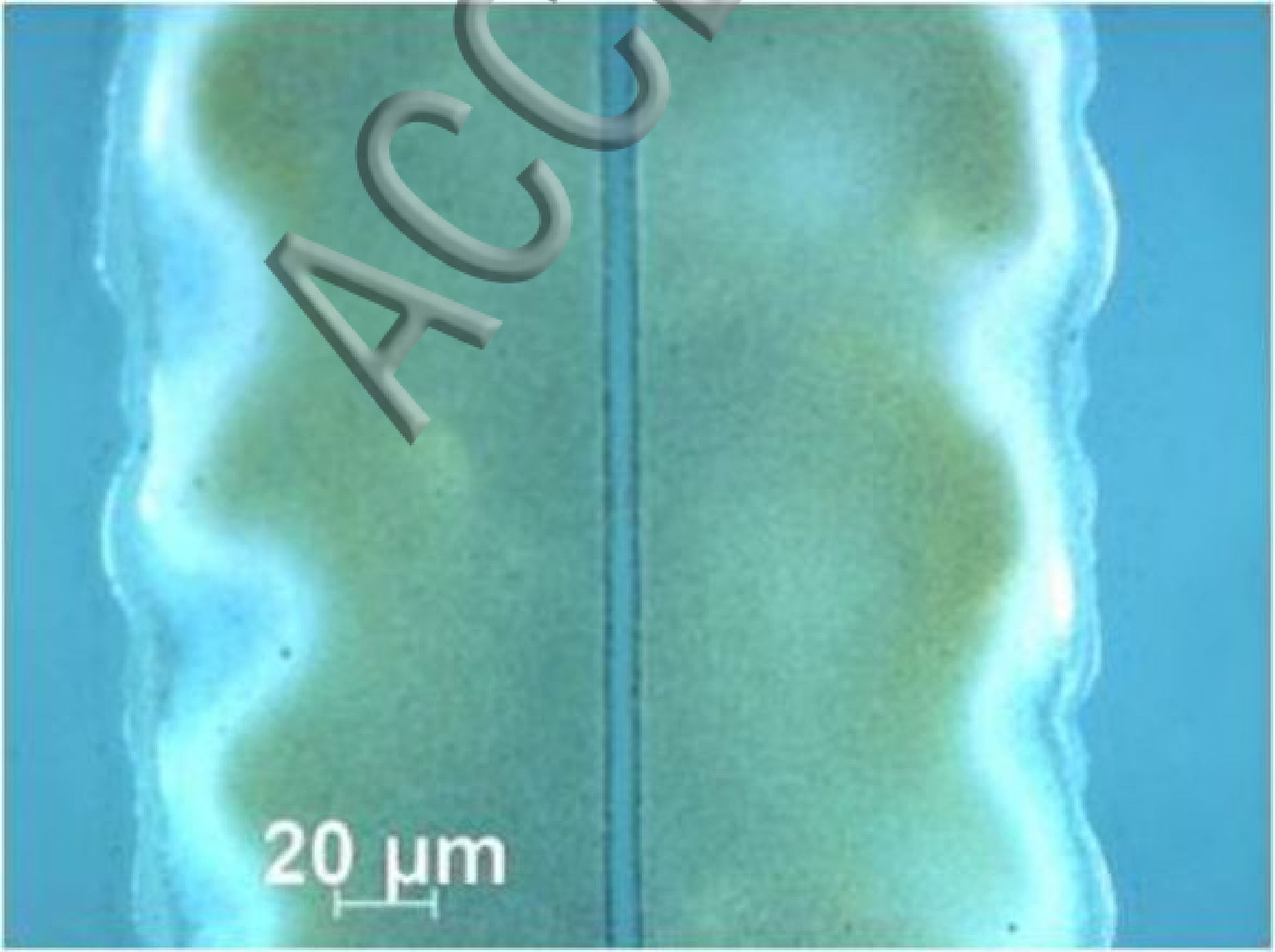
20 µm

4.66 μm

П